Engineering Structures 183 (2019) 30–51

Contents lists available at ScienceDirect

Engineering Structures

journal homepage: www.elsevier.com/locate/engstruct

Static and dynamic analysis of corrugated-core sandwich plates using finite strip method

Hossein Zamanifar, Saeid Sarrami-Foroushani, Mojtaba Azhari*

Department of Civil Engineering, Isfahan University of Technology, Isfahan 84156-83111, Iran

ARTICLE INFO

Keywords:
Corrugated-core sandwich plate
Static analysis
Free vibration
Forced vibration
Finite strip method
First order shear deformation theory

ABSTRACT

Free and forced vibration and static analysis of corrugated-core sandwich plates are investigated in this study by employing the classic finite strip method. The 3D corrugated-core plate is converted to a 2D orthotropic continuum model by considering some equivalent elastic constants. Various boundary conditions and different features of these plates are explored and the geometric and mechanical factors influencing their responses, such as displacements, rotations, moments and shear forces, are evaluated. Because of the significant effect of the shear stiffness on the behavior of corrugated-core sandwich plates, the first order shear deformation theory (FSDT) is used to analyze the plate. Due to the comparatively low shear to flexural stiffness ratio of these plates compared to ordinary plates, the convergence of the results is relatively slow. Therefore, a fast numerical technique such as finite strip method which yields effective reduction of calculation cost is employed. A MATLAB program is developed to obtain the results and the validity of the proposed method is evaluated by comparing the results with those presented by previous researches.

1. Introduction

Corrugated-core sandwich plate (CSP) is a three-layered composite structure that consists of two main parts: a corrugated sheet (called the core plate) in the middle of the sandwich plate which has a sinus or trapezoidal cross section composed of high-strength or soft material, and two rectangular flat thin sheets that are connected to the top and bottom of the core, called the face plates. These plates are generally made up of high-strength materials such as steel or carbon fiber.

Corrugated sandwich plates can be widely used in construction industries because of their simple handling and manufacturing compared with other types of composite plates. Some of the advantages of CSPs are as follows:

- By increasing the gap between the two face plates and placing the core between them, the section moment of inertia and the load capacity of the structure also increase.
- The weight of CSP decreases due to the presence of empty spaces in the core. These spaces also provide the possibility of passing the facilities.
- The ability to absorb and deplete energy increases by using different materials in cores.
- Carrying and installing CSPs is easier than ordinary plates.
- The ability to isolate heat and sound in such plates is reachable by embedding insulating materials as core plate or in the middle of empty spaces of the plate. It is notable that corrugated core sandwich plates are periodic structures, which are capable of developing the wave stop bands (or band gaps) that acts like a directional frequency filter which restricts the free propagation of elastic/acoustic waves [1–4]. This effect can reduce the noise or vibration to some extent.

Considering performance and economical aspects, the above mentioned features make the CSPs an ideal choice for using as slabs or shear walls in structures. The most important obstacle against the widespread usage of these plates in structures is the difficulty and the expenses of welding of the joining plates. If an appropriate connection between the constituent plates is not provided, the core and face plates cannot operate as a single integrated unit and this may cause serious damages to the structure. The difference between the cross section of the core in two orthogonal directions (x and y) results in different flexural and shear behavior in these two directions, which generally makes the skeleton of the entire plate similar to the orthotropic ones.

The first theoretical works on structural sandwich constructions were published by Gough et al. [5] and Williams et al. [6]. The applicable theories of flat sandwich plates with small deformations were

* Corresponding author.
E-mail address: mojtaba@cc.iut.ac.ir (M. Azhari).

https://doi.org/10.1016/j.engstruct.2018.12.102
Received 13 October 2018; Received in revised form 22 December 2018; Accepted 30 December 2018

proposed by Libove and Batdorf [7]. Based on the dual behavior of these plates in their orthogonal directions, Hubka and Libove [8] proposed some elastic constants for reducing 3D sandwich plate to a two-dimensional orthotropic equivalent continuum. This detailed paper laid the foundation for further researches in this field. Their method has proper precision and gives close results to experimental tests. In this approach, the governing equations of the CSPs are obtained by simulating them with continuous orthotropic structures. Caillerie et al. [9] and Bourgeois et al. [10] examined periodic plates by studying one cell of the entire plate and presented their homogenization methods. By changing the core shape, one can achieve different properties. Fung et al. [11,12] investigated the C-core and Z-core sandwich plates and derived elastic constants for modeling these kinds of sandwich plates. He et al. [13] presented a semi-analytical method for bending analysis of corrugated-core, honeycomb-core and X-core sandwich panels. They determined the maximum deflection of these plates by employing Fourier series and the Galerkin approach along with the finite element analysis. In their paper, the discrete geometric nature of the core is taken into account by considering the core plates as beams and the sandwich panel as composite structure consists of plates and beams with proper displacement compatibility. Lok et al. [14] proposed elastic constants for a truss-core sandwich plate and presented a closed form solution along with the 3D finite element modeling. These plates are very much alike the corrugated-core sandwich plates. The main difference in their sections is the absence of horizontal part in the section of truss-core sandwich plate which separates the elements of the core plate. Liang et al. [15] presented an optimal design for corrugated plates exposed to blast loads. Chang et al. [16] analyzed corrugate sandwich plates using the first order shear deformation theory for the equivalent orthotropic thick plate. Using Navier's method, they presented an elasto-plastic analysis of CSPs with different geometric parameters. Buannic et al. [17] and Biancolini [18] investigated the bending behavior of CSP using homogenization and finite element methods. Isaksson et al. [19] mathematically divided the corrugated panel into a number of thin layers each of which possesses a unique effective elastic modulus. The layers are then assembled in order to analyze the corrugated panels as a plate with equivalent mechanical properties. To reduce the anisotropic performance of the structure, Seong et al. [20] introduced a kind of bi-directional corrugated plate which showed quasi-isotropic behaviors in bending. Different methods have been proposed by researchers for modeling the CSPs or calculating the elastic constants. Bartolozzi et al. [21] proposed a general analytical method for obtaining the equivalent constants for various corrugation geometries. Also, Boorle et al. [22] studied the influence of some geometric parameters on the bending and displacement of a truss-core plate with all simply supported boundary conditions. The vibration of a simply supported truss-core sandwich plate was investigated by Lok et al. using a double series solution to obtain closed form results [23]. Free vibration analysis of corrugated-core sandwich plates was done by Peng et al. [24] using a meshfree Galerkin method based on the first order shear deformation theory. The corrugated-core sandwich plates have a low weight to strength ratio due to their hollow structure. Because of the broad application of these plates in building and ship structures and different industrial tools, choosing the optimal geometric characteristics for them is an important issue. Also, the dynamic behavior of CSPs is a sensitive matter due to their empty spaces which reduce the total density of the plate and eventually affect the dynamic response of the CSP.

Numerous numerical methods are developed over the years for static and dynamic analysis of plates, through which the finite element and finite strip methods are the most powerful ones. The finite strip method employs fewer degrees of freedom rather than FEM and provides more efficient formulations for plate analysis under different loads and boundary conditions. Moreover, the speed of the method when using a large number of harmonic terms and elements is a sensible advantage. As it will be discussed later in the paper, employing higher terms of harmonic series in CSPs is inevitable to achieve the desired convergence.

In this paper, free and forced vibration and static analysis of corrugated-core sandwich plates subjected to static and dynamic out of plane loadings are investigated by developing the finite strip method based on first order shear deformation theory. The effect of several geometric and mechanical parameters on maximum displacements of the corrugated-core sandwich plates is presented in order to approach an efficient design. Also, the convergence of the results, displacements curves, bending moment, transverse shear and rotation diagrams, FRF[1] graphs along with the free vibration diagrams of CSPs with various geometric factors and different boundary conditions are parametrically studied. To the best knowledge of the authors, the finite strip method is employed for the first time to analyze the CSPs, including a comprehensive study on diverse boundary conditions in static and dynamic problems. The FRF diagrams of CSPs, which are not considered elsewhere, are also presented in this paper.

2. Theory

The required relations for modeling the corrugated-core sandwich plate as well as the finite strip formulation based on first order shear deformation theory are presented in this section.

2.1. Equivalent elastic constants

Consider a corrugated-core sandwich plate in a Cartesian coordinate and its equivalent orthotropic plate as shown in Fig. 1a and b, respectively. The bending stiffness along the x-axis, called the strong direction, represented by D_x is obtained as follows:

$$D_x = E_f I_f + E_c I_c \tag{1}$$

in which, E_f and E_c are the elastic moduli of the face plates and core plate, respectively. Also, I_f and I_c are the moments of inertia of the cross section for the face plate and core plate, respectively. These moments of inertia are defined as:

$$I_f = P t_f h^2 + \frac{P t_f^3}{3} \tag{2}$$

$$I_c = \frac{f\, t_c h_c^2}{2} + \frac{t_c h_c^3}{6\sin(\theta)} + \frac{f\, t_c^3}{6} \tag{3}$$

The parameters of Eqs. (2) and (3) which are schematically shown in Fig. 2a are defined as follows:

P: the half-width of each unit (one corrugation)
t_f: face plate thickness
t_c: core plate thickness
f: the length of horizontal part of the core plate including the arced parts (crown)
θ: the corrugation (or inclination) angle
h_c: the depth of the corrugation, equals to the distance from center to center of the horizontal parts of core plate (web height).
h: the depth of the plate, equals to the distance from center to center of the face plates.

The bending stiffness along the y-axis, called the weak direction, represented by D_y is also calculated from Eq. (4):

$$D_y = \frac{E_f I_f}{1 - \nu_f^2\left(1 - \frac{E_f I_f}{D_x}\right)} \tag{4}$$

in which the ν_f is the Poisson's ratio of the face plates.

[1] Frequency Response Function

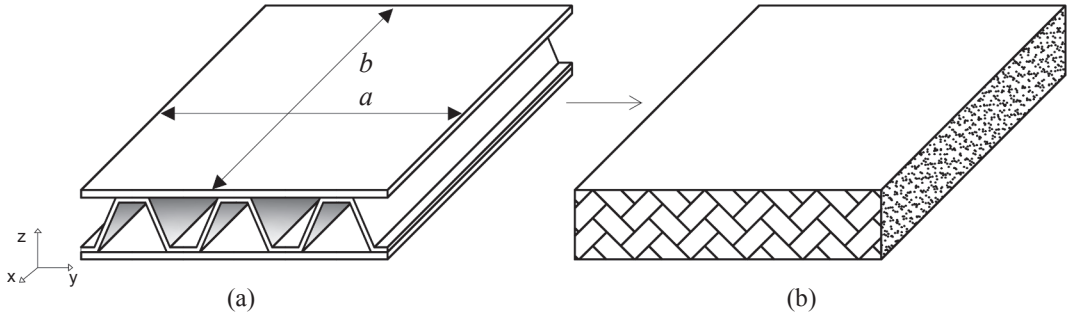

Fig. 1. An overview of converting a CSP to equivalent orthotropic plate: (a) corrugated-core sandwich plate and (b) Equivalent orthotropic plate.

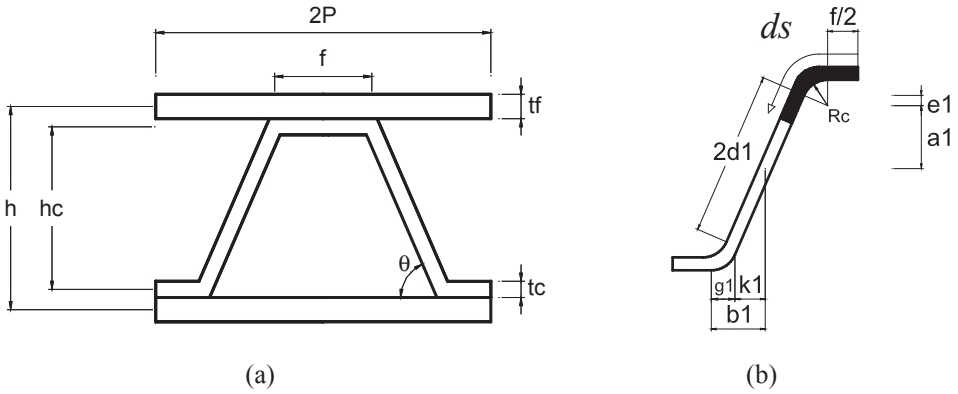

Fig. 2. The view of one unit of corrugated-core sandwich plate in y-z plane.

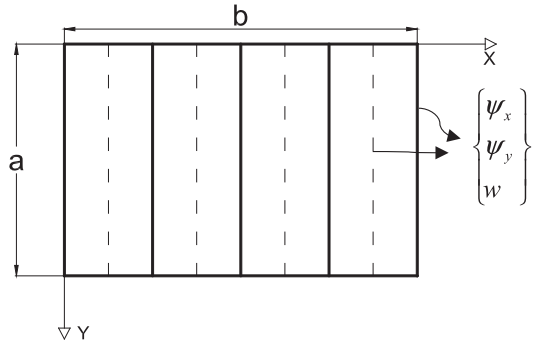

Fig. 3. An overview of dividing a plate with length a and width b into finite strips.

Table 1
Boundary conditions at plate edges.

	$x = 0$ or $x = b$				$y = 0$ or $y = a$			
B.Cs	ψ_x	ψ_y	w	M_x	ψ_x	ψ_y	w	M_y
Simple (S)	–	0	0	0	0	–	0	0
Clamped (C)	0	0	0	–	0	0	0	–
Free (F)	–	–	–	0	–	–	–	0
Guided (G)	0	0	–	–	0	0	–	–

The twisting stiffness, D_{xy}, is also obtained as follows:

$$D_{xy} = 2G_f I_f \tag{5}$$

in which G_f is the shear modulus of the face plates. Note that in order to use I_f and I_c in Eqs. (1), (4), and (5), they must be considered for one unit of the length and therefore they have to be divided by $2P$.

The transverse shear stiffness in the planes perpendicular to the corrugation axis, D_{qy}, is given by Eq. (6):

$$D_{qy} = Sh\left(\frac{E_c}{1-\nu_c^2}\right)\left(\frac{t_c}{h_c}\right)^3 \tag{6}$$

where ν_c is the Poisson's ratio of the core plate. Moreover, S is a non-dimensional parameter which could be calculated based on the relations presented in the Appendix (see also Fig. 2b).

The transverse shear stiffness in the planes parallel to the corrugation axis, D_{qx}, is given by:

$$D_{qx} = \frac{G_c I t_c h}{P\int_0^L Q ds} \tag{7}$$

in which G_c is the shear modulus of the core plate. I is the total moment of inertia and Q is the static moment about the neutral axis of $2P$ width of the cross section parallel to y-z plane. Also, L is the length of one corrugation leg and the integral is calculated on one leg of the corrugation.

In most cases the contribution of the core for carrying the bending moment is negligible, so it could be assumed that the entire bending moment is tolerated by the face plates. The assumption which states that the normal stresses induced by bending, solely apply on the face plates results in a constant shear flow in the section. Therefore, the values of I, Q, and consequently D_{qx} are approximately calculated as follows:

$$I \approx Pt_f h^2 \tag{8a}$$

$$\int_0^L Q ds \approx Pt_f hL \tag{8b}$$

$$D_{qx} = \frac{G_c I t_c h}{P\int_0^L Q ds} \approx \frac{G_c(Pt_f h^2)t_c h}{P(Pt_f hL)} = \frac{G_c t_c h^2}{PL} \tag{8c}$$

The shear stiffness constants presented by Libove and Hubka [8] directly connects the shear stresses to the rotations caused by them. Hence, the shear correction factor in FSDT is not required in the calculations. In fact, their method does not consider the shear stress

Table 2
Convergence study of maximum deflection (mm) for different inclination angles and different number of harmonic terms (m).

m	B.Cs/Angle					
	SSSS			CCCC		
	50°	70°	90°	50°	70°	90°
1	0.0033425	0.0058327	0.0076371	0.0016140	0.0031115	0.0037829
3	0.0032553	0.0053573	0.0066929	0.0015386	0.0025656	0.0028004
5	0.0032702	0.0054752	0.0069808	0.0016240	0.0028411	0.0032635
7	0.0032653	0.0054302	0.0068564	0.0016086	0.0027123	0.0030057
9	0.0032675	0.0054517	0.0069204	0.0016366	0.0028062	0.0031725
11	0.0032663	0.0054399	0.0068836	0.0016300	0.0027506	0.0030594
13	0.0032670	0.0054471	0.0069065	0.0016438	0.0027972	0.0031428
15	0.0032666	0.0054424	0.0068914	0.0016402	0.0027665	0.0030804
17	0.0032669	0.0054456	0.0069018	0.0016484	0.0027942	0.0031300
19	0.0032667	0.0054433	0.0068943	0.0016461	0.0027748	0.0030907
21	0.0032668	0.0054450	0.0068999	0.0016516	0.0027931	0.0031233
23	0.0032667	0.0054437	0.0068957	0.0016499	0.0027797	0.0030964
25	0.0032668	0.0054447	0.0068990	0.0016539	0.0027927	0.0031195
27	0.0032667	0.0054439	0.0068964	0.0016527	0.0027829	0.0030999
29	0.0032668	0.0054446	0.0068985	0.0016556	0.0027927	0.0031171
31	0.0032667	0.0054440	0.0068967	0.0016547	0.0027852	0.0031022
33	0.0032668	0.0054445	0.0068982	0.0016569	0.0027927	0.0031156
35	0.0032667	0.0054441	0.0068970	0.0016562	0.0027869	0.0031039
$\frac{D_{qy}}{D_y}$	54.8	5.3	1.6	54.8	5.3	1.6
$\frac{D_{qx}}{D_x}$	44.1	34.9	28.4	44.1	34.9	28.4
α(%)	2.27	6.66	9.69	−2.62	10.43	17.95

Table 3
Maximum deflections of corrugated-core sandwich plate.

θ (deg)	$\frac{h_c}{t_c}$	$\frac{t_c}{t_f}$	$\frac{P}{h_c}$	w(mm)	
				Ref. [16]	Present study
60	10	0.6	1	0.095	0.0947
		1	1.2	0.191	0.1910
		1.25	1.4	0.280	0.2795
70	20	0.6	1	0.640	0.6388
		1	1.2	1.312	1.3114
		1.25	1.4	1.948	1.9476

Table 4
Bending moments at the center of the of corrugated-core sandwich plate.

θ (deg)	$\frac{t_c}{t_f}$	$\frac{P}{h_c}$	Ref. [16]		Present study	
			$M_x\left(\frac{\text{kN·m}}{\text{m}}\right)$	$M_y\left(\frac{\text{kN·m}}{\text{m}}\right)$	$M_x\left(\frac{\text{kN·m}}{\text{m}}\right)$	$M_y\left(\frac{\text{kN·m}}{\text{m}}\right)$
60	0.6	1	1.91	5.16	1.907	5.158
	1	1.2	2.01	5.14	2.011	5.135
	1.25	1.4	2.12	5.10	2.129	5.096
70	0.6	1	2.05	5.07	2.051	5.067
	1	1.2	2.19	5.04	2.199	5.039
	1.25	1.4	2.35	4.99	2.365	4.982

Table 5
Natural frequencies of isotropic plate for five different modes ($t/b = 0.1$).

a/b	Reference	Mode number				
		1	2	3	4	5
1	Present study	1.9317	4.6083	4.6089	7.0718	8.6158
	Ref. [31]	1.9317	4.6084	4.6084	7.0716	8.6162
2.5	Present study	1.1364	1.5936	2.3396	3.3533	3.8829
	Ref. [31]	1.1364	1.5936	2.3397	3.3533	3.8826

distribution as a constant stress but the shear strain distribution is considered linear just like the FSDT. It is also possible to define equivalent flexural and shear moduli for the hypothetical orthotropic plate by equating the equations presented in Ref. [8] with the relationships used to calculate the elastic constants of an ordinary plate. Using equations presented in this section, the CSP is converted to an equivalent orthotropic plate.

2.2. Displacement field

The Reissner-Mindlin [25,26] plate theory, also known as the first order shear deformation theory, states that each section of the plate remains straight but not necessarily orthogonal to the middle plane after deformation. This assumption makes it possible to use C^0 continuous elements, thus there is no need to satisfy the first derivative of variables in boundary conditions. In fact, since the FSDT takes the shear deformations of the plate into account, the total rotation in a section will be the sum of bending and shear rotations and can be considered as an independent variable.

The displacement field associated with this theory consists of two in-plane components, u, v and one out of plane component, w. The total rotations about the y and x axis are represented by $\psi_x(x, y)$ and $\psi_y(x, y)$, respectively and the vertical out of plane displacement is shown by $w_0(x, y)$. Therefore, the displacement field is expressed as:

$$u(x, y, z) = u_0(x, y) + z\psi_x(x, y) \tag{9a}$$

$$v(x, y, z) = v_0(x, y) + z\psi_y(x, y) \tag{9b}$$

$$w(x, y, z) = w_0(x, y) \tag{9c}$$

in which $\psi_x(x, y)$ and $\psi_y(x, y)$are defined as:

$$\psi_x(x, y) = \phi_x - \frac{\partial w_0}{\partial x} \tag{10a}$$

$$\psi_y(x, y) = \phi_y - \frac{\partial w_0}{\partial y} \tag{10b}$$

where ϕ_x and ϕ_y are shear rotations and $-\partial w_0/\partial x$ and $-\partial w_0/\partial y$ are bending rotations.

Table 6
Effect of R_c on the equivalent elastic constants and the maximum displacement of the corrugated-core sandwich plate.

R_c/h_c	w (mm)	D_x (N·m)	D_y (N·m)	D_{xy} (N·m)	D_{qx} (N/m)	D_{qy} (N/m)
0	0.1675	1.918×10^7	1.528×10^7	1.152×10^7	7.303×10^8	2.107×10^8
0.03	0.1672	1.918×10^7	1.528×10^7	1.152×10^7	7.333×10^8	2.130×10^8
0.06	0.1668	1.918×10^7	1.528×10^7	1.152×10^7	7.364×10^8	2.162×10^8
0.09	0.1664	1.918×10^7	1.528×10^7	1.152×10^7	7.394×10^8	2.204×10^8
0.12	0.1659	1.918×10^7	1.528×10^7	1.152×10^7	7.425×10^8	2.255×10^8
0.15	0.1653	1.918×10^7	1.528×10^7	1.152×10^7	7.456×10^8	2.315×10^8
0.18	0.1647	1.918×10^7	1.528×10^7	1.152×10^7	7.487×10^8	2.383×10^8

Table 7
Effect of P on the equivalent elastic constants and maximum displacement of the corrugated-core sandwich plate.

P/h_c	w (mm)	D_x (N·m)	D_y (N·m)	D_{xy} (N·m)	D_{qx} (N/m)	D_{qy} (N/m)
1	0.1649	1.918×10^7	1.528×10^7	5.760×10^6	7.477×10^8	2.359×10^8
1.2	0.1916	1.934×10^7	1.529×10^7	5.760×10^6	5.515×10^8	1.055×10^8
1.4	0.2299	1.946×10^7	1.529×10^7	5.760×10^6	4.240×10^8	5.856×10^7
1.6	0.2786	1.955×10^7	1.530×10^7	5.760×10^6	3.363×10^8	3.717×10^7
1.8	0.3368	1.962×10^7	1.530×10^7	5.760×10^6	2.734×10^8	2.571×10^7
2	0.4032	1.968×10^7	1.531×10^7	5.760×10^6	2.267×10^8	1.887×10^7

Table 8
Effect of the inclination angle on the equivalent elastic constants and maximum displacement of the corrugated-core sandwich plate.

θ (deg)	w (mm)	Dx (N·m)	Dy (N·m)	Dxy (N·m)	Dqx (N/m)	Dqy (N/m)
50	0.1493	1.808×10^7	1.521×10^7	1.152×10^7	7.967×10^8	8.329×10^8
55	0.1535	1.865×10^7	1.525×10^7	1.152×10^7	7.716×10^8	4.956×10^8
60	0.1649	1.918×10^7	1.528×10^7	1.152×10^7	7.477×10^8	2.359×10^8
65	0.1824	1.966×10^7	1.530×10^7	1.152×10^7	7.247×10^8	1.302×10^8
70	0.2053	2.013×10^7	1.533×10^7	1.152×10^7	7.027×10^8	8.184×10^7
75	0.2331	2.058×10^7	1.535×10^7	1.152×10^7	6.814×10^8	5.629×10^7
80	0.2651	2.102×10^7	1.537×10^7	1.152×10^7	6.608×10^8	4.121×10^7
85	0.3010	2.146×10^7	1.539×10^7	1.152×10^7	6.408×10^8	3.156×10^7
90	0.3406	2.191×10^7	1.542×10^7	1.152×10^7	6.213×10^8	2.498×10^7

Table 9
Comparison between the cross section area of CSP and ordinary plate with the same maximum deflection.

h_c (m)	w(mm)	A(cm^2)	
		CSP	Ordinary plate
0.1	0.225	86	229
0.12	0.165	88	254
0.14	0.124	90	282
0.16	0.095	92	306

2.3. Finite strip method

The finite strip method is based on a mathematical approximation of the exact solution of the problem. The method was first proposed by Cheung [27] for analyzing simple structures. Over the years, through the development of more advanced forms of the finite strip method, it became a powerful and fast tool for investigating more complex structures [28,29]. However, the domain of the problems covered by FSM is more limited than FEM. In this method, the plate is divided into a number of strips in transverse direction. By applying the FSDT to this method, each strip has three nodal lines and every nodal line has three unknown coefficients (Fig. 3). The displacement field of the plate is estimated by two kinds of functions:

a. Continuous harmonic series that satisfy the transverse boundary conditions of the plate
b. Polynomial interpolation functions in transverse direction

Since the problem has C^0-continuity in this study, the Lagrange shape functions are used to interpolate in-plane and out of plane displacements in the transverse direction. From now on, as shown in Fig. 3, the width of plate is assumed to be along the transverse direction (x-axis) which is divided into strips while the length is the dimension along the harmonic shape functions (along y-axis in Fig. 3). Therefore, each variable can be estimated as:

$$\psi_x(x,y) = \sum_{n=1}^{r}\sum_{i=1}^{3} C_i\psi_{xi}Y_n = \sum_{n=1}^{r}(C_1\psi_{x1} + C_2\psi_{x2} + C_3\psi_{x3})Y_n = \sum_{n=1}^{r}[C][\psi_x]Y_n = \sum_{n=1}^{r}[N_n][\psi_x] \tag{11a}$$

$$\psi_y(x,y) = \sum_{n=1}^{r}\sum_{i=1}^{3} C_i\psi_{yi}U_n = \sum_{n=1}^{r}(C_1\psi_{y1} + C_2\psi_{y2} + C_3\psi_{y3})U_n = \sum_{n=1}^{r}[C][\psi_y]U_n = \sum_{n=1}^{r}[M_n][\psi_y] \tag{11b}$$

$$w(x,y) = \sum_{n=1}^{r}\sum_{i=1}^{3} C_i w_i Y_n = \sum_{n=1}^{r}(C_1 w_1 + C_2 w_2 + C_3 w_3)Y_n = \sum_{n=1}^{r}[C][w]Y_n = \sum_{n=1}^{r}[N_n][w] \tag{11c}$$

in which

$$[N_n] = [N_{n1}, N_{n2}, N_{n3}] = [C_1Y_n, C_2Y_n, C_3Y_n]$$
$$[M_n] = [M_{n1}, M_{n2}, M_{n3}] = [C_1U_n, C_2U_n, C_3U_n] \tag{12}$$

where C_1 to C_3 are Lagrange shape functions and can be written as:

$$C_1(x) = \frac{2x^2}{b_s^2} - \frac{3x}{b_s} + 1 \tag{13a}$$

$$C_2(x) = \frac{4x}{b_s} - \frac{4x^2}{b_s^2} \tag{13b}$$

Table 10
Maximum deflection of CSPs for different web thicknesses and inclination angles (t_f = 1 cm).

θ (deg)	t_c (mm)	w (mm)	D_x (N·m)	D_y (N·m)	D_{xy} (N·m)	D_{qx} (N/m)	D_{qy} (N/m)
50	6	0.1658	1.585×10^7	1.414×10^7	1.076×10^7	4.467×10^8	4.112×10^8
	8	0.1562	1.696×10^7	1.467×10^7	1.114×10^7	6.163×10^8	6.304×10^8
	10	0.1493	1.808×10^7	1.521×10^7	1.152×10^7	7.967×10^8	8.329×10^8
	12	0.1435	1.920×10^7	1.575×10^7	1.191×10^7	9.882×10^8	1.020×10^9
	14	0.1383	2.033×10^7	1.630×10^7	1.230×10^7	1.191×10^9	1.201×10^9
	16	0.1335	2.147×10^7	1.686×10^7	1.270×10^7	1.405×10^9	1.380×10^9
	18	0.1291	2.262×10^7	1.743×10^7	1.311×10^7	1.632×10^9	1.560×10^9
	20	0.1249	2.377×10^7	1.800×10^7	1.352×10^7	1.870×10^9	1.744×10^9
60	6	0.2374	1.651×10^7	1.419×10^7	1.076×10^7	4.192×10^8	6.027×10^7
	8	0.1875	1.784×10^7	1.473×10^7	1.114×10^7	5.784×10^8	1.295×10^8
	10	0.1649	1.918×10^7	1.528×10^7	1.152×10^7	7.477×10^8	2.359×10^8
	12	0.1518	2.052×10^7	1.583×10^7	1.191×10^7	9.274×10^8	3.852×10^8
	14	0.1430	2.187×10^7	1.639×10^7	1.230×10^7	1.118×10^9	5.773×10^8
	16	0.1362	2.323×10^7	1.695×10^7	1.270×10^7	1.319×10^9	8.067×10^8
	18	0.1307	2.460×10^7	1.752×10^7	1.311×10^7	1.531×10^9	1.065×10^9
	20	0.1258	2.597×10^7	1.810×10^7	1.352×10^7	1.755×10^9	1.343×10^9
70	6	0.4130	1.709×10^7	1.423×10^7	1.076×10^7	3.940×10^8	1.884×10^7
	8	0.2658	1.860×10^7	1.478×10^7	1.114×10^7	5.436×10^8	4.278×10^7
	10	0.2053	2.013×10^7	1.533×10^7	1.152×10^7	7.027×10^8	8.184×10^7
	12	0.1749	2.166×10^7	1.589×10^7	1.191×10^7	8.715×10^8	1.407×10^8
	14	0.1570	2.320×10^7	1.645×10^7	1.230×10^7	1.050×10^9	2.237×10^8
	16	0.1453	2.475×10^7	1.702×10^7	1.270×10^7	1.240×10^9	3.340×10^8
	18	0.1367	2.631×10^7	1.760×10^7	1.311×10^7	1.439×10^9	4.736×10^8
	20	0.1300	2.788×10^7	1.818×10^7	1.352×10^7	1.649×10^9	6.431×10^8
80	6	0.6643	1.762×10^7	1.426×10^7	1.076×10^7	3.705×10^8	8.955×10^6
	8	0.3812	1.932×10^7	1.481×10^7	1.114×10^7	5.112×10^8	2.103×10^7
	10	0.2651	2.102×10^7	1.537×10^7	1.152×10^7	6.608×10^8	4.121×10^7
	12	0.2089	2.273×10^7	1.594×10^7	1.191×10^7	8.197×10^8	7.214×10^7
	14	0.1779	2.445×10^7	1.651×10^7	1.230×10^7	9.879×10^8	1.165×10^8
	16	0.1589	2.618×10^7	1.708×10^7	1.270×10^7	1.166×10^9	1.769×10^8
	18	0.1460	2.792×10^7	1.766×10^7	1.311×10^7	1.353×10^9	2.557×10^8
	20	0.1366	2.966×10^7	1.825×10^7	1.352×10^7	1.551×10^9	3.549×10^8
90	6	0.9522	1.815×10^7	1.429×10^7	1.076×10^7	3.484×10^8	5.222×10^6
	8	0.5237	2.003×10^7	1.485×10^7	1.114×10^7	4.806×10^8	1.255×10^7
	10	0.3406	2.191×10^7	1.542×10^7	1.152×10^7	6.213×10^8	2.498×10^7
	12	0.2524	2.380×10^7	1.598×10^7	1.191×10^7	7.707×10^8	4.417×10^7
	14	0.2048	2.570×10^7	1.655×10^7	1.230×10^7	9.288×10^8	7.184×10^7
	16	0.1764	2.760×10^7	1.713×10^7	1.270×10^7	1.096×10^9	1.098×10^8
	18	0.1580	2.952×10^7	1.771×10^7	1.311×10^7	1.272×10^9	1.597×10^8
	20	0.1451	3.144×10^7	1.830×10^7	1.352×10^7	1.458×10^9	2.233×10^8

$$C_3(x) = \frac{2x^2}{b_s^2} - \frac{x}{b_s} \tag{13c}$$

in which b_s is the width of each strip. Also $Y_n = Y_n(y)$ is the shape function along the longitudinal direction corresponding to nth mode and U_n is the first derivative of Y_n. The function Y_n are assumed $\sin\frac{n\pi y}{a}$ and $\sin\frac{n\pi y}{a}\sin\frac{\pi y}{a}$ for simply supported and clamped edges, respectively. The composition of the variables for nth mode for formulating the computer program is as follows:

$$\psi_x(x, y) = [N_{n1}\ \ 0\ \ 0\ \ N_{n2}\ \ 0\ \ 0\ \ N_{n3}\ \ 0\ \ 0][\psi_x] \tag{14a}$$

$$\psi_y(x, y) = [0\ \ M_{n1}\ \ 0\ \ 0\ \ M_{n2}\ \ 0\ \ 0\ \ M_{n3}\ \ 0][\psi_y] \tag{14b}$$

$$w\ (x, y) = [0\ \ 0\ \ N_{n1}\ \ 0\ \ 0\ \ N_{n2}\ \ 0\ \ 0\ \ N_{n3}][w] \tag{14c}$$

Unknown vectors $[\psi_x]$, $[\psi_y]$and $[w]$ for each strip are written as:

$$[\psi_x] = [\psi_{x1}\ \ 0\ \ 0\ \ \psi_{x2}\ \ 0\ \ 0\ \ \psi_{x3}\ \ 0\ \ 0]^T \tag{15a}$$

$$[\psi_y] = [0\ \ \psi_{y1}\ \ 0\ \ 0\ \ \psi_{y2}\ \ 0\ \ 0\ \ \psi_{y3}\ \ 0]^T \tag{15b}$$

$$[w] = [0\ \ 0\ \ w_1\ \ 0\ \ 0\ \ w_2\ \ 0\ \ 0\ \ w_3]^T \tag{15c}$$

2.3.1. Static analysis

The strain energy, U, for an elastic strip can be calculated as:

$$U = \frac{1}{2}\int_0^a \int_0^{b_s} \delta^T \mathbf{B}^T \mathbf{D}\mathbf{B}\delta\, dxdy \tag{16}$$

in which, **B** and **D** are strain and property matrices, respectively and δ is the displacement vector.

Also, the potential energy, V, due to the external lateral load, $P_z(x, y)$, can be written as:

$$V = \int_0^a \int_0^{b_s} \delta^{\mathbf{T}} \mathbf{N}^{\mathbf{T}} P_z(x, y)\, dxdy \tag{17}$$

in which **N** denotes the shape function vector which consists of all terms of series expansion.

The total potential energy of the plate, Π, is defined as:

$$\Pi = V + U \tag{18}$$

The principle of the minimum potential energy requires that:

$$\frac{\partial \Pi}{\partial \delta} = \int_0^a \int_0^{b_s} \mathbf{B}^T \mathbf{D}\mathbf{B}\delta\, dxdy - \int_0^a \int_0^{b_s} \mathbf{N}^T P_z(x, y)\, dxdy = \mathbf{0} \tag{19}$$

According to Eq. (19), one can define the stiffness matrix and load vector for each strip corresponding mth and nth modes.

$$\mathbf{F}_n = \int_0^a \int_0^{b_s} \mathbf{N}_n^T P_z(x, y)\, dxdy \tag{21}$$

$$\mathbf{K}_{mn} = \int_0^a \int_0^{b_s} \mathbf{B}_m^T \mathbf{D}\mathbf{B}_n\, dxdy \tag{20}$$

The strain matrix for mth mode, $\mathbf{B}_m^T$, is written as:

Table 11
Maximum deflection of CSPs for different face thicknesses and inclination angles (t_c = 1 cm).

θ (deg)	t_f (mm)	w (mm)	D_x (N·m)	D_y (N·m)	D_{xy} (N·m)	D_{qx} (N/m)	D_{qy} (N/m)
50	6	0.2615	1.150×10^7	8.605×10^6	6.459×10^6	7.445×10^8	8.304×10^8
	8	0.1912	1.468×10^7	1.181×10^7	8.911×10^6	7.704×10^8	8.330×10^8
	10	0.1493	1.808×10^7	1.521×10^7	1.152×10^7	7.967×10^8	8.329×10^8
	12	0.1215	2.167×10^7	1.882×10^7	1.429×10^7	8.235×10^8	8.378×10^8
	14	0.1018	2.549×10^7	2.264×10^7	1.722×10^7	8.507×10^8	8.500×10^8
	16	0.0871	2.952×10^7	2.667×10^7	2.032×10^7	8.784×10^8	8.687×10^8
	18	0.0757	3.377×10^7	3.093×10^7	2.359×10^7	9.065×10^8	8.925×10^8
	20	0.0666	3.825×10^7	3.541×10^7	2.704×10^7	9.350×10^8	9.199×10^8
60	6	0.2825	1.260×10^7	8.656×10^6	6.459×10^6	6.987×10^8	1.892×10^8
	8	0.2092	1.578×10^7	1.187×10^7	8.911×10^6	7.229×10^8	2.122×10^8
	10	0.1649	1.918×10^7	1.528×10^7	1.152×10^7	7.477×10^8	2.359×10^8
	12	0.1353	2.277×10^7	1.889×10^7	1.429×10^7	7.728×10^8	2.580×10^8
	14	0.1143	2.659×10^7	2.271×10^7	1.722×10^7	7.983×10^8	2.772×10^8
	16	0.0986	3.062×10^7	2.675×10^7	2.032×10^7	8.243×10^8	2.934×10^8
	18	0.0866	3.487×10^7	3.101×10^7	2.359×10^7	8.507×10^8	3.073×10^8
	20	0.0771	3.935×10^7	3.549×10^7	2.704×10^7	8.775×10^8	3.196×10^8
70	6	0.3301	1.355×10^7	8.694×10^6	6.459×10^6	6.566×10^8	6.842×10^7
	8	0.2532	1.674×10^7	1.191×10^7	8.911×10^6	6.794×10^8	7.489×10^7
	10	0.2053	2.013×10^7	1.533×10^7	1.152×10^7	7.027×10^8	8.184×10^7
	12	0.1727	2.373×10^7	1.895×10^7	1.429×10^7	7.263×10^8	8.871×10^7
	14	0.1491	2.754×10^7	2.277×10^7	1.722×10^7	7.503×10^8	9.507×10^7
	16	0.1315	3.157×10^7	2.681×10^7	2.032×10^7	7.747×10^8	1.008×10^8
	18	0.1177	3.582×10^7	3.107×10^7	2.359×10^7	7.995×10^8	1.059×10^8
	20	0.1067	4.030×10^7	3.556×10^7	2.704×10^7	8.247×10^8	1.106×10^8
80	6	0.3961	1.444×10^7	8.725×10^6	6.459×10^6	6.175×10^8	3.604×10^7
	8	0.3159	1.763×10^7	1.195×10^7	8.911×10^6	6.390×10^8	3.856×10^7
	10	0.2651	2.102×10^7	1.537×10^7	1.152×10^7	6.608×10^8	4.121×10^7
	12	0.2296	2.462×10^7	1.899×10^7	1.429×10^7	6.830×10^8	4.384×10^7
	14	0.2035	2.843×10^7	2.282×10^7	1.722×10^7	7.056×10^8	4.631×10^7
	16	0.1834	3.246×10^7	2.687×10^7	2.032×10^7	7.286×10^8	4.861×10^7
	18	0.1675	3.671×10^7	3.113×10^7	2.359×10^7	7.519×10^8	5.074×10^7
	20	0.1545	4.120×10^7	3.562×10^7	2.704×10^7	7.756×10^8	5.275×10^7
90	6	0.4770	1.533×10^7	8.753×10^6	6.459×10^6	5.806×10^8	2.258×10^7
	8	0.3941	1.852×10^7	1.199×10^7	8.911×10^6	6.008×10^8	2.377×10^7
	10	0.3406	2.191×10^7	1.542×10^7	1.152×10^7	6.213×10^8	2.498×10^7
	12	0.3024	2.551×10^7	1.904×10^7	1.429×10^7	6.422×10^8	2.617×10^7
	14	0.2736	2.932×10^7	2.287×10^7	1.722×10^7	6.634×10^8	2.732×10^7
	16	0.2509	3.335×10^7	2.692×10^7	2.032×10^7	6.850×10^8	2.842×10^7
	18	0.2323	3.760×10^7	3.119×10^7	2.359×10^7	7.069×10^8	2.948×10^7
	20	0.2168	4.209×10^7	3.568×10^7	2.704×10^7	7.292×10^8	3.051×10^7

Table 12
Maximum deflections (mm) of the CSPs for different mechanical properties of face and core plates.

Case	1		2		3		4	
E_f (GPa)	208		208		70		70	
E_c(GPa)	208		70		208		70	
a/b	θ (deg)		θ (deg)		θ (deg)		θ (deg)	
	60	90	60	90	60	90	60	90
0.5	0.0014	0.0042	0.0031	0.0086	0.0022	0.0060	0.0041	0.0124
1	0.0041	0.0069	0.0074	0.0125	0.0079	0.0105	0.0122	0.0204
1.5	0.0061	0.0076	0.0100	0.0134	0.0119	0.0119	0.0180	0.0225
2	0.0071	0.0077	0.0112	0.0134	0.0138	0.0123	0.0210	0.0228
2.5	0.0076	0.0076	0.0118	0.0132	0.0146	0.0124	0.0225	0.0227
3	0.0078	0.0076	0.0120	0.0130	0.0149	0.0124	0.0231	0.0226
3.5	0.0079	0.0076	0.0121	0.0129	0.0150	0.0124	0.0234	0.0225
4	0.0079	0.0075	0.0122	0.0128	0.0150	0.0124	0.0236	0.0224
4.5	0.0079	0.0075	0.0122	0.0127	0.0150	0.0124	0.0236	0.0223
5	0.0079	0.0075	0.0122	0.0127	0.0150	0.0123	0.0236	0.0223

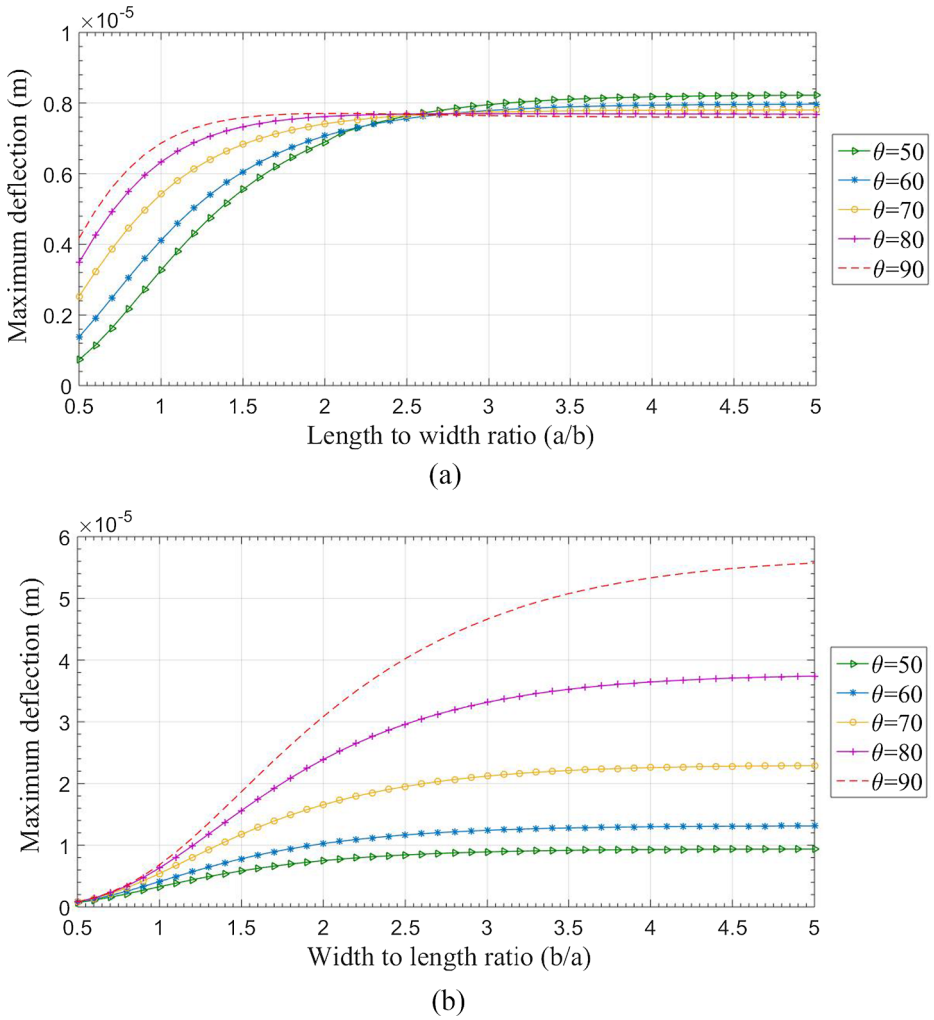

Fig. 4. Maximum transverse deflection of SSSS CSPs for different inclination angles, (a) Constant width, and (b) Constant length.

$$\mathbf{B}_m = [\mathbf{B}_{m1} \quad \mathbf{B}_{m2} \quad \mathbf{B}_{m3}] \tag{22}$$

in which $\mathbf{B}_{mi}$ is:

$$\mathbf{B}_{mi} = \begin{bmatrix} \frac{\partial N_{mi}}{\partial x} & 0 & 0 \\ 0 & \frac{\partial M_{mi}}{\partial y} & 0 \\ \frac{\partial N_{mi}}{\partial y} & \frac{\partial M_{mi}}{\partial x} & 0 \\ N_{mi} & 0 & \frac{\partial N_{mi}}{\partial x} \\ 0 & M_{mi} & \frac{\partial N_{mi}}{\partial y} \end{bmatrix} \qquad i = 1, 2, 3 \tag{23}$$

and

$$\mathbf{N}_n = [N_{n1} \;\; 0 \;\; 0 \;\; N_{n2} \;\; 0 \;\; 0 \;\; N_{n3} \;\; 0 \;\; 0] \tag{24}$$

Also the property matrix, $\mathbf{D}$, can be found in Eq. (25):

$$\mathbf{D} = \begin{bmatrix} \frac{D_x}{1-\nu_x\nu_y} & \frac{\nu_y D_x}{1-\nu_x\nu_y} & 0 & 0 & 0 \\ \frac{\nu_x D_y}{1-\nu_x\nu_y} & \frac{D_y}{1-\nu_x\nu_y} & 0 & 0 & 0 \\ 0 & 0 & 0.5D_{xy} & 0 & 0 \\ 0 & 0 & 0 & D_{qx} & 0 \\ 0 & 0 & 0 & 0 & D_{qy} \end{bmatrix} \tag{25}$$

The Poisson's ratio associated with bending along x-direction, ν_x, is equal to face plates Poisson's ratio, ν_f, while it is equal to $\nu_x D_y/D_x$ along y-direction.

The total stiffness matrix, $\mathbf{K}^t$, and loading vector, $\mathbf{F}^t$, of the plate is achieved after assembling stiffness matrices and load vectors corresponding to different modes, taking the boundary conditions into account. The equilibrium equation can be finally formed as:

$$\mathbf{K}^t\boldsymbol{\delta}_{st} - \mathbf{F}^t = \mathbf{0} \tag{26}$$

Displacement vector of the plate can be achieved by Eq. (27)

$$\boldsymbol{\delta}_{st} = (\mathbf{K}^t)^{-1}\mathbf{F}^t \tag{27}$$

The bending moments and shear forces in a CSP are now obtained as follows:

$$M_{xx} = \frac{D_x}{1-\nu_x\nu_y}\left(\frac{\partial \psi_x}{\partial x} + \nu_y\frac{\partial \psi_y}{\partial y}\right) \tag{28a}$$

$$M_{yy} = \frac{D_y}{1-\nu_x\nu_y}\left(\frac{\partial \psi_y}{\partial y} + \nu_x\frac{\partial \psi_x}{\partial x}\right) \tag{28b}$$

$$M_{xy} = 0.5D_{xy}\left(\frac{\partial \psi_y}{\partial x} + \frac{\partial \psi_x}{\partial y}\right) \tag{28c}$$

$$Q_{xz} = D_{qx}\left(\psi_x + \frac{\partial w_0}{\partial x}\right) \tag{28d}$$

$$Q_{yz} = D_{qy}\left(\psi_y + \frac{\partial w_0}{\partial y}\right) \tag{28e}$$

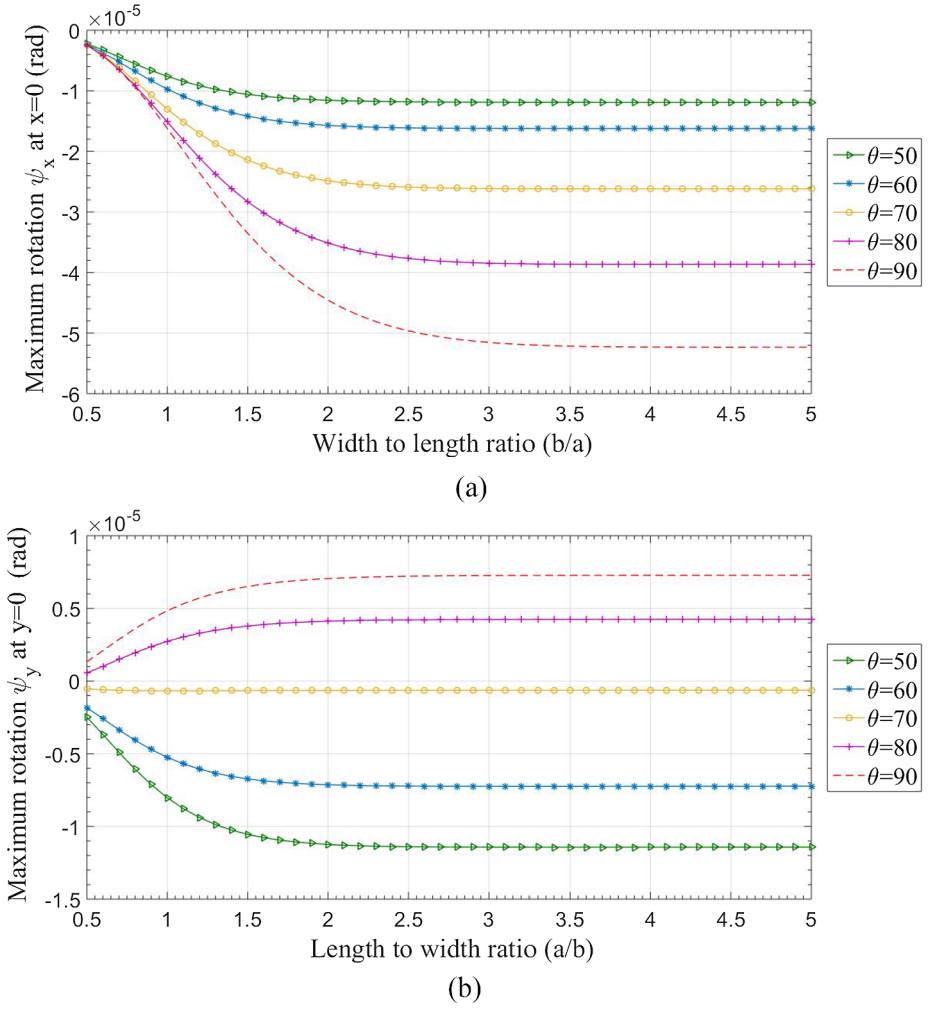

Fig. 5. Rotation at the edges of SSSS CSPs for different inclination angles and aspect ratios, (a) ψ_x and (b) ψ_y.

2.3.2. Vibration analysis

The total energy of a vibrating plate without damping is the sum of kinetic, strain, and potential energies:

$$\Pi = T + U + V \tag{29}$$

In the case of free vibration, the term V will vanish. The kinetic energy, T, in the Mindlin theory is expressed by Eq. (30):

$$T = \iint_A \frac{\rho h^3}{24}\left[\left(\frac{\partial \psi_x}{\partial t}\right)^2 + \left(\frac{\partial \psi_y}{\partial t}\right)^2\right] + \frac{\rho h}{2}\left(\frac{\partial w}{\partial t}\right)^2 dxdy \tag{30}$$

in which ρ is the density of the plate and ψ_x, ψ_y and w are the functions of coordinates and time. By a similar process to static analysis, the mass submatrix, $\mathbf{M}_{mn}$ for a single strip is obtained by Eq. (31):

$$\mathbf{M}_{mn} = \int_0^a \int_0^{b_s} \mathbf{B}_{vm}^T \mathbf{P} \mathbf{B}_{vn} dxdy \tag{31}$$

in which

$$\mathbf{B}_{vm} = [\mathbf{B}_{vm1} \quad \mathbf{B}_{vm2} \quad \mathbf{B}_{vm3}] \tag{32}$$

and

$$\mathbf{B}_{vmi} = \begin{bmatrix} N_{mi} & 0 & 0 \\ 0 & M_{mi} & 0 \\ 0 & 0 & N_{mi} \end{bmatrix} \quad i = 1, 2, 3 \tag{33}$$

The density matrix, $\mathbf{P}$, is defined as:

$$\mathbf{P} = \begin{bmatrix} \frac{\rho h_t^3}{12} & 0 & 0 \\ 0 & \frac{\rho h_t^3}{12} & 0 \\ 0 & 0 & \rho h_t \end{bmatrix} \tag{34}$$

h_t in Eq. (34) is the total height of the plate. Since the structure of the corrugated-core sandwich plates is hollow, the density of the constitutive material of the plate is different from the overall density of the structure. Therefore, it is necessary to define an equivalent density for analyzing the 2D orthotropic plate. By forming the total stiffness matrix ($\mathbf{K}^t$) and total mass matrix ($\mathbf{M}^t$) and solving an eigenvalue problem, the natural frequencies of the plate is obtained.

$$|\mathbf{K}^t - \omega_n^2 \mathbf{M}^t| = \mathbf{0} \tag{35}$$

When the plate is vibrating under dynamic loadings, $P(x, y, t_1)$, the displacement vector is calculated by Duhamel's integral. If the load function is separated to static and dynamic parts, e. g., $P(x, y, t_1) = P_0(x, y) f(t_1)$, the displacements can be calculated from:

$$\delta = \delta_{st} \omega_n \int_0^t f(t_1) \sin(\omega_n (t - t_1)) dt_1 \tag{36}$$

in which the static displacement vector, δ_{st}, is defined in Eq. (27).

3. Boundary conditions

Since the elements of the plate in FSDT have C^0-continuity, the chosen displacement field should satisfy the boundary conditions of

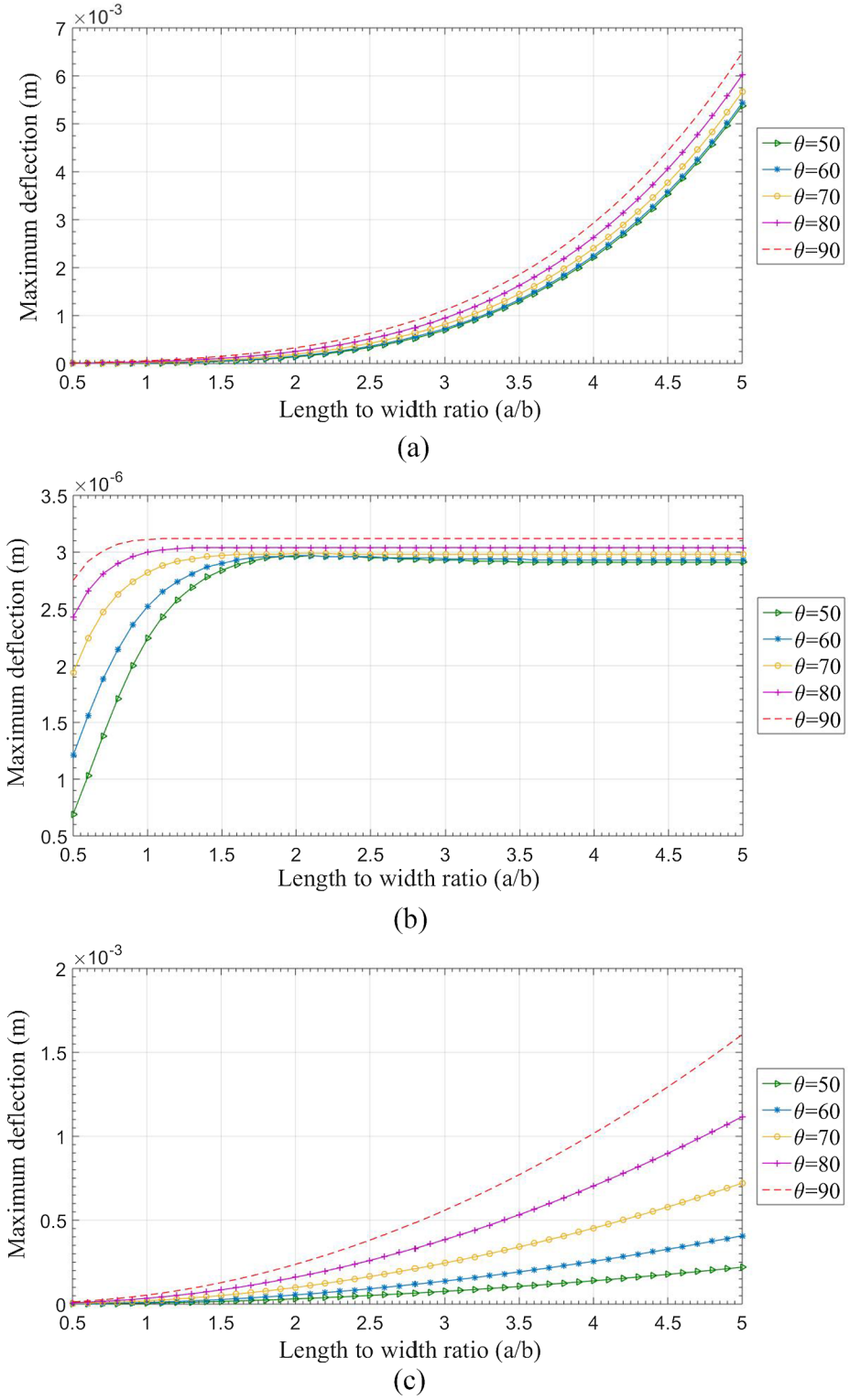

Fig. 6. Maximum transverse deflection of CSPs versus aspect ratio for different inclination angles and (a) FSFS, (b) CSCS, and (c) GSGS boundary conditions.

zero order. As stated, the transverse boundary conditions of the plate are satisfied by using continuous harmonic functions. In general, different boundary conditions in the longitudinal or transverse direction at $y = 0$ or $y = a$ and $x = 0$ or $x = b$ should be satisfied as shown in Table 1.

4. Numerical results

In most cases of this study, both of face and core plates are assumed to be made of structural steel. The typical structural elastic modulus can be considered between 200 and 220 GPa. In this study, the modulus of elasticity of steel is assumed to be 208 GPa. The elastic modulus of aluminum in one of the examples is supposed to be 70 GPa. The poisson's ratio for both core and face plates in all of the cases is assumed to

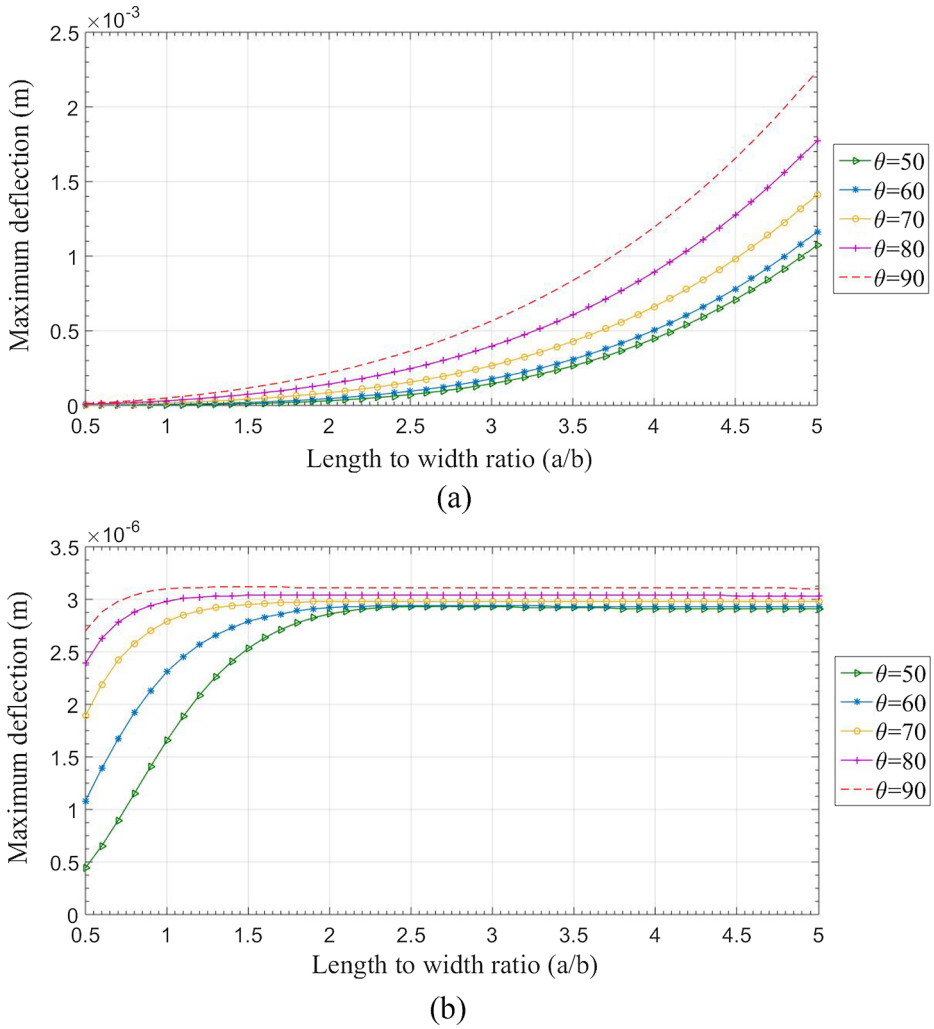

Fig. 7. Maximum transverse deflection of CSPs versus aspect ratio for different inclination angles and (a) FCFC (b) CCCC boundary conditions.

be 0.3 and the steel density is 7800 kg/m^3. Material properties can be found in [16,30]. In the matter of boundary conditions, the first letter corresponds to the left edge of the plate. The next letters are assigned in a counter-clockwise manner. In all sections, the plate is under uniformly distributed loading of 10 kN/m^2. Wherever the geometric parameters are not mentioned specifically, they are taken as follows:

$t_c = t_f = 1\,\text{cm}$, $h_c = P = 10\,\text{cm}$, $R_c = 1.7\,\text{cm}$, $\theta = 60°$

Several codes are developed in MATLAB environment for static and dynamic analyzing of corrugated-core sandwich plates. Since the mass and stiffness matrices usually have large dimensions due to the employing numerous harmonic series and strips, the Gaussian quadrature rules are used as a numerical method of integration. Many numerical examples and results are provided using these codes.

4.1. Convergence study

In order to reach the proper convergence of the proposed method, the number of strips and terms of harmonic series should be considered. In an ordinary plate in which shear to flexural stiffness ratios have relatively large values, the number of strips and harmonic series mostly depend on the aspect ratio, thickness to dimensions ratio, and the boundary conditions. But, due to the hollow structure of the corrugated-core sandwich plates, the shear to flexural stiffness ratio is relatively small compared with the ordinary plates. The effect of relatively low shear stiffness is similar to the effect of increasing the height of an ordinary plate in which the shear deformations and the number of required harmonic terms increase. Therefore, the convergence process in analyzing of CSPs depends on the geometry of the plate cross section as well. Every parameter which decreases the shear stiffnesses, D_{qx} and D_{qy}, will slow down the speed of convergence.

Static analysis of a square, 1 m length CSP is now considered to evaluate the convergence of the proposed method. Three inclination angles and different number of harmonic series are assumed and maximum deflections of the plate are presented in Table 2. The parameter α in Table 2 is the percentage of difference between the first and the last answers. It is observed that bigger inclination angle which provides less shear stiffness, requires more harmonic terms for convergence. Also, it is evident that the convergence rate of SSSS boundary conditions is faster than CCCC boundary conditions. In this paper, the number of harmonic terms and strips are chosen so that the difference between two successive answers does not exceed 1%.

4.2. Verification

To validate the proposed method, the values of maximum deflections along with the bending moments at the center of the CSPs are presented in Tables 3 and 4, respectively. The results are then compared to those of Ref. [16], in which a SSSS CSP with $a = 2.1$ m, $b = 6$ m, and $h_c = 0.1$ m is studied using the Navier's method. It can be seen that the results are in good agreement with those presented in Ref. [16]. To obtain the results of Tables 2 and 3, the required elastic constants are

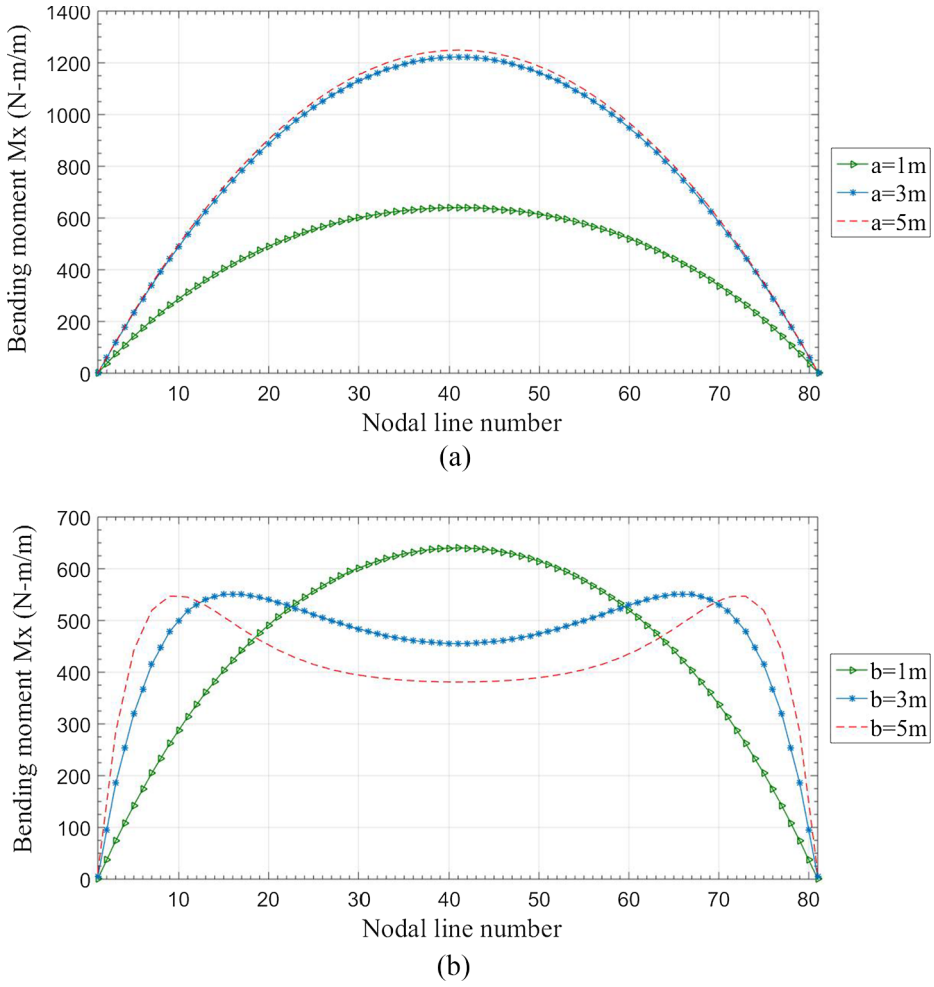

Fig. 8. Bending moment M_x in the middle of all edges simply supported CSPs along the transverse direction: (a) Constant width, and (b) Constant length.

assumed exactly equal to what is supposed in [16]. However, the constants used in our study are calculated more exactly.

As for the vibration analysis, a non-dimensional frequency factor, λ, defined in Eq. (37) is calculated for orthotropic plate.

$$\lambda = \frac{\omega_n b^2}{\pi^2}\sqrt{\frac{\rho h_t (1-\nu_x\nu_y)}{D_x}} \tag{37}$$

in which, ω_n is the minimum natural frequency of the plate and other parameters are already defined. For isotropic plates, we have $D_x = Eh_t^3/12$ and $\nu_x = \nu_y = \nu$.

The non-dimensional frequency factor is calculated for isotropic plates using the proposed finite strip method. The results are presented in Table 5 as well as those reported in Ref. [31]. It could be observed from Table 5 that the FSM results are in good agreement with those of Ref. [31].

4.3. Static analysis

In this section, a comprehensive parametric study on the static analysis of CSPs with different geometric parameters and boundary conditions is presented in three subsections.

4.3.1. Effect of geometric and mechanical parameters

The effect of geometric and mechanical parameters in the cross section of CSPs with SSSS boundary conditions on the equivalent constants and maximum deflection of the plate is investigated in this section. The plate is under uniformly distributed loading and all calculations are done for $a = 2.1$ m and $b = 6$ m, except in sections *d* and *f*. Maximum deflections of CSP are calculated and the results are presented in Tables 6 to 12 which are being described in the following:

4.3.1.1. Effect of "R_c". This parameter affects the length of corrugation leg (L) and the dimensionless coefficient, S introduced in Section 2.1. As it is observed in Table 6, the change in the length of the core's arc at the joint of horizontal and inclined parts of the web, has a very slight and negligible effect on the flexural constants. However, by increasing R_c in the section, the shear elastic constants slightly increase and therefore the displacements are reduced.

4.3.1.2. Effect of "P". In spite of the slight increase in D_x and D_y due to the increase of the horizontal part of the core plate, increasing the ratio of P/h_c leads to decrease of the shear stiffness constants, especially D_{qy}, and consequently increasing the deformation of the CSP. Meanwhile, by increasing the distance between the elements of the core parts (legs and crowns) and the relative reduction of used materials in a certain length, the overall stiffness of the plate decreases, and consequently, the out of plane displacements are increased. The equivalent elastic constants along with the corresponding displacement at the center of the CSP with $h_c = 0.1$ m and different values of P/h_c are presented in Table 7.

4.3.1.3. Effect of "θ". Besides the thickness and dimensions of the plates, the most effective parameter in the function of a corrugated sandwich plate is the inclination angle of the core plate. This angle affects the geometry of the plate and consequently influences the equivalent constants. Although the changes in the angle of inclination partly influence the flexural stiffnesses, the shear stiffness constant, D_{qy},

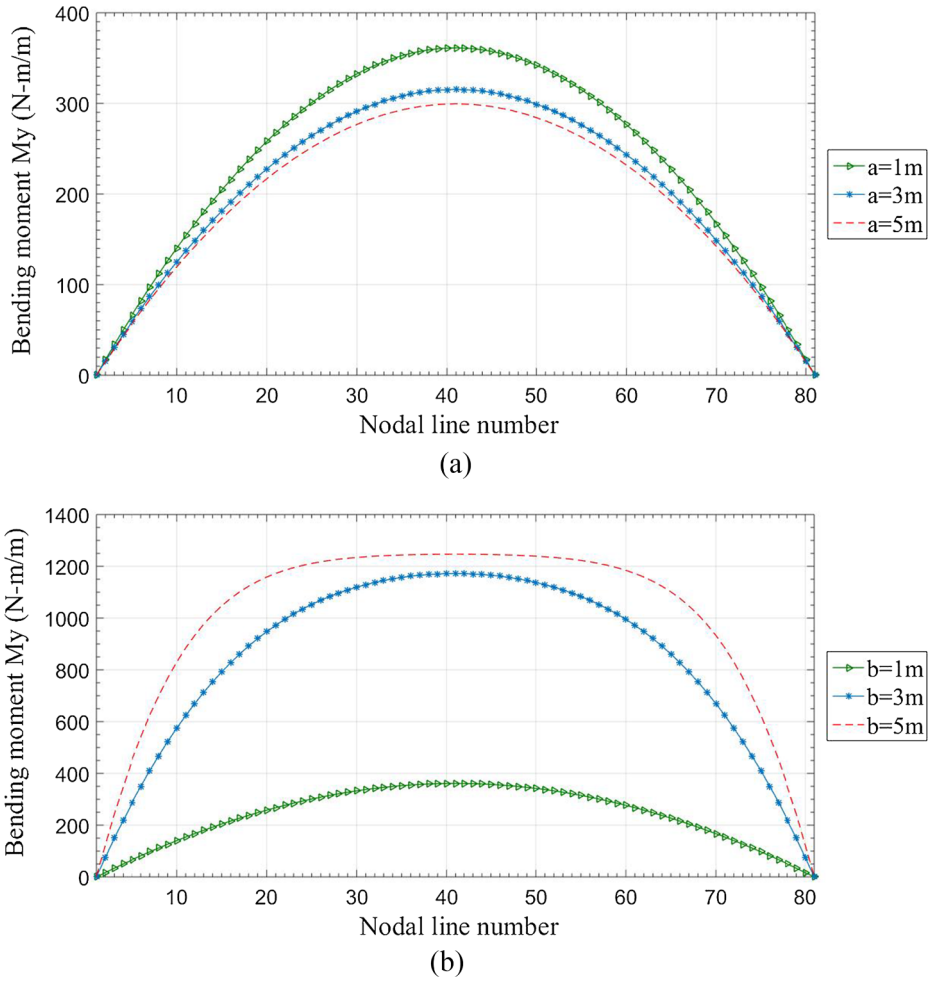

Fig. 9. Bending moment M_y in the middle of all edges simply supported CSPs along the transverse direction: (a) Constant width, and (b) Constant length.

is greatly affected by the variation of this parameter. The significant reduction of D_{qy} due to increasing the angle of inclination will result in a considerable increase in the out of plane displacements. The values of the equivalent elastic constants along with the corresponding displacement at the center of the plate are presented in Table 8.

4.3.1.4. Effect of "h_c". Table 9 presents the maximum deflections of square CSPs with different web heights, h_c. The length of the plate is equal to 3 m, and $P = 12.5$ cm. Also, the cross sectional area of one unit of the CSP is compared to the area of an ordinary plate with the width of 2P for a constant central deflection. The results clearly demonstrate the economic efficiency of corrugated sandwich plates.

4.3.1.5. Effect of "t_c" and "t_f". The effect of thickness of the core and face plates are studied in this section. The maximum transverse deflection of CSPs for different web thicknesses ($t_f = 1$ cm) and five inclination angles are presented in Table 10. The effects of the thickness of face sheets in a CSP with $t_c = 1$ cm are considered in Table 11. It is observed that changing the face plate thickness has more considerable reducing effect on the displacements, but in large inclination angles, like 90°, the increase in core thickness can also be weighty in abating the deflections. It is reminded that in many cases, increasing the face plate thickness leads to larger cross section area of the plate and consequently the higher costs of the CSP.

4.3.1.6. Effect of mechanical properties. The effect of mechanical properties of the CSPs on the maximum displacement of a plate with 1 m width is considered in this section. The core and face sheets are supposed to be made of steel and aluminum. Four different cases are considered and the results are presented in Table 12. As expected, the displacements in Case 1 are less than the other cases, while the Case 4 yields higher values of displacements. It appears that for inclination angle of 60°, the maximum displacements in Case 3 are higher than Case 2 (except for $a/b = 0.5$), while for the angle of 90°, Case 2 yields higher deflections in the plate. The displacements in Cases 2 and 3 for angle 90°, and in Case 2 for angle 60° are approximately the same for higher aspect ratios. Therefore, using stronger material in the core (or face) plate, will not necessarily yields more economic design in practical purposes.

4.3.2. Maximum deflections and rotations of CSP

The deformation of CSPs is investigated in this section. Different boundary conditions are considered and the results are presented in Figs. 4 to 7.

4.3.2.1. SS transverse edges. The diagrams of maximum deflection of SSSS CSP for different length to width (a/b) and width to length (b/a) ratios are plotted in Fig. 4 for five corrugation angles. As it is shown in Fig. 4a, by increasing the length to width ratio the displacements at the center of the plate converge to approximately equal values. Although this process can not necessarily be called convergence, it can be concluded that by increasing the spacing between the supports, and consequently reducing the stiffness of the middle regions, the role of other effective parameters such as inclination angle of the web becomes somehow insignificant. Generally, the smaller angle of inclination causes the smaller displacement of the plate. However, it can be seen

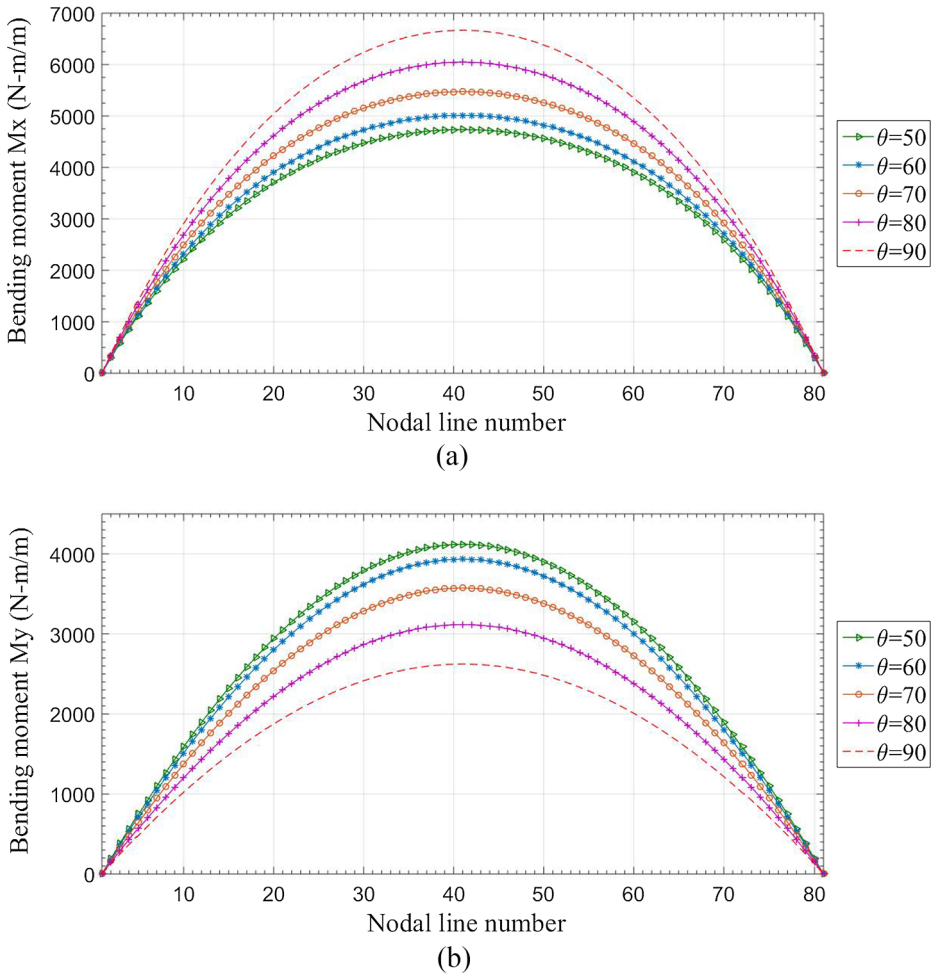

Fig. 10. Variations of bending moment in the middle of all edges simply supported CSPs along the transverse direction for different inclination angles: (a) M_x, and (b) M_y.

that by exceeding the length to width ratio from a certain value, the displacement of CSP with smaller angles will be slightly higher than the larger angles. This issue does not appear in Fig. 4b. In addition, in most aspect ratios, the displacements in Fig. 4b have higher values than Fig. 4a. This is mainly due to the difference of properties and stiffnesses of the CSP in two orthogonal directions. Also just like beams and slabs, the dimensions of the plate is a significant factor and in this type of orthotropic plate, increasing the dimensions in each direction will affect the results differently.

Assume that the higher stiffnesses of the plate are along the transverse direction (x-axis). By increasing the width of the plate, the main resistance factor in the plate is weakened while the other direction will not undergo a great reduction in stiffness. Hence, the displacements are higher in Fig. 4b. By increasing the length of the plate, the larger stiffnesses along the strong directions are less affected and can still operate more effectively than the other direction and consequently the results do not vary too much in higher values of a/b ratios. It seems that the effects of other parameters, such as bigger flexural stiffness constants for larger inclinations angles, lead to smaller displacements in the higher lengths of Fig. 4a.

Fig. 5a and 5b show the rotations of CSPs for different values of lengths and widths. As shown in Fig. 5a, the maximum rotation in longitudinal boundaries (ψ_x) increase by increasing the inclination angle. However, the rotations remain approximately constant after certain values of the width. The constant pattern of the results is also observed in Fig. 5b for ψ_y, but the point in this graph is the different sign of the rotations in transverse boundaries for angles 80° and 90° rather than the other three angles which could be attributed to the smaller shear to flexural stiffness in these conditions. This phenomenon can affect the sign of the $M_y$in some cases.

In Fig. 6a–c, the diagrams of maximum deflection of CSP for different aspect ratios and inclination angles are plotted for FSFS, CSCS and GSGS boundary conditions, respectively. As for FSFS case, as the length of the plate (and consequently the length of the free boundaries) increases, the freedom of the longitudinal boundaries (along the y-axis) allows the central out of plane displacements to grow unlimitedly. In fact, as the length of the plate increases in this arrangement of boundary conditions, the plate behavior becomes closer to a simply supported beam.

As shown in Fig. 6b, the displacements at the center of a CSCS CSP, for high aspect ratios, are approximately 40 percent of the corresponding ones in a CSP with SSSS boundary conditions shown in Fig. 4a. Moreover, the trend of convergence of displacements begins from smaller aspect ratios for CSCS, compared with the SSSS case.

The difference between FSFS and GSGS boundary conditions, which are shown in Fig. 6a and c, respectively, is due to the restriction of rotations at the longitudinal boundaries of the CSP for GSGS boundary conditions. Since the effect of transverse displacements on the behavior of the plate is usually more determinative than nodal rotations, the overall shape of the displacement curves for GSGS and FSFS boundary conditions are similar. However, the values of displacements for GSGS plate will grow with slower slope than FSFS.

4.3.2.2. CC transverse edges. The variation of maximum displacements

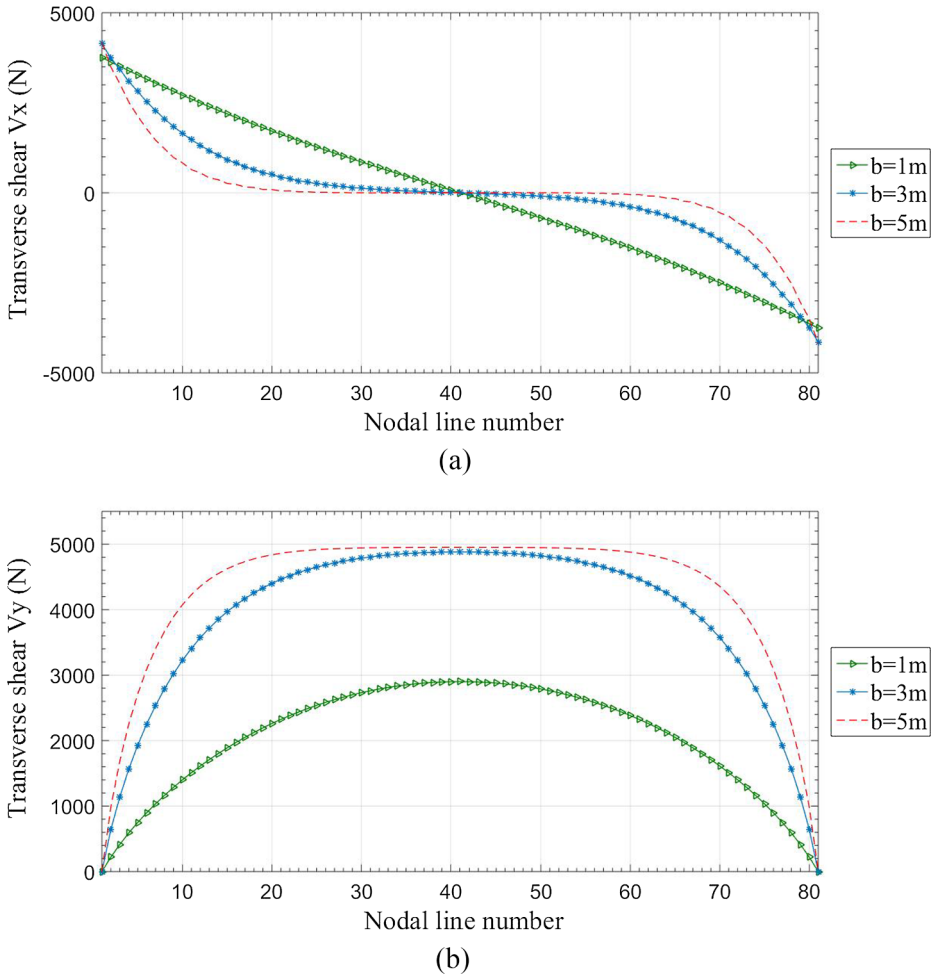

Fig. 11. Transverse shear of all edges simply supported CSPs along the transverse direction for different widths and constant length: (a) V_x@ y = a/2, and (b) V_y@ y = 0 or y = a.

of CSPs with FCFC and CCCC boundary conditions are demonstrated in Fig. 7a and 7b. As for the FCFC case in Fig. 7a, the displacements can increase unlimitedly but with smaller values than FSFS case. For CCCC boundary conditions in Fig. 7b, all displacements and rotations are restricted at all four edges, and as a result, the displacements will become the smallest. The displacements of CCCC CSPs for high aspect ratios are very close to CSCS case. While for the smaller values of aspect ratios, the results of CCCC boundary conditions are lower and as the inclination angles increases, the difference between these two cases begin to fade, even for small length to width ratios.

4.3.3. Bending moment and shear force diagrams

4.3.3.1. SS transverse edges. Bending moment diagrams in the middle of the corrugated sandwich plates with the specifications mentioned before are presented in this section. Because of the orthotropic behavior of the CSP, the moment variations in x and y directions are different even in a square plate. The length and width which are not mentioned specifically in the graphs are equal to 1 m.

The bending moment diagrams of SSSS CSPs in the strong direction for different lengths and widths are illustrated in Fig. 8a and b, respectively. By increasing the length of the plate, the moments in the strong direction take higher values (Fig. 8a). This growth in the moments becomes more intangible as the length of the plate increases. It can be seen that if the width of the plate increases (Fig. 8b), the moment diagrams will tend to appear in the form of a saddle. The reason is the spacing of the longitudinal supports which weakens the plate in its strong direction and hence reduces the support effects on the middle areas of the plate that are supposed to bend in this direction. This will make the distant areas from the supports softer and eventually, it causes the reduction of developed bending moments in x direction in these regions.

The bending moments of SSSS CSPs in the weak direction are also shown in Fig. 9a and b for different values of lengths and widths, respectively. As observed, like the previous example, there is the same correlation between the direction of the moments and dimensions of the plate. Increasing the length will yield lower bending moments and increasing the width will upraise them.

Moreover, the effect of inclination angle on the bending moment diagrams is considered in this section. The variations of M_x and M_y in the middle line of steel CSPs with $a = b = 3$ m, and five different inclination angles are illustrated in Fig. 10a and b, respectively. Unlike Fig. 10a, the bending moment developed in the middle of the plate ($y = a/2$) takes smaller values for larger angles as shown in Fig. 10b. Therefore, considering this fact that the difference in the inclination angles loses its effect on the amount of displacements by increasing the length to width ratio (as shown in Fig. 4a), one can consider the reduction of the bending moment M_y as one of the advantages of using larger angles.

The variation of transverse shear force parallel to y-z plane, V_x, in the middle ($y = a/2$) of a CSP is shown in Fig. 11a, while the transverse shear force diagram parallel to x-z plane, V_y, in the transverse supports ($y = 0$ or $y = a$) of a corrugated sandwich plate with variable widths, is shown in Fig. 11b.

Fig. 12a shows the bending moment diagrams, M_x, in the middle of

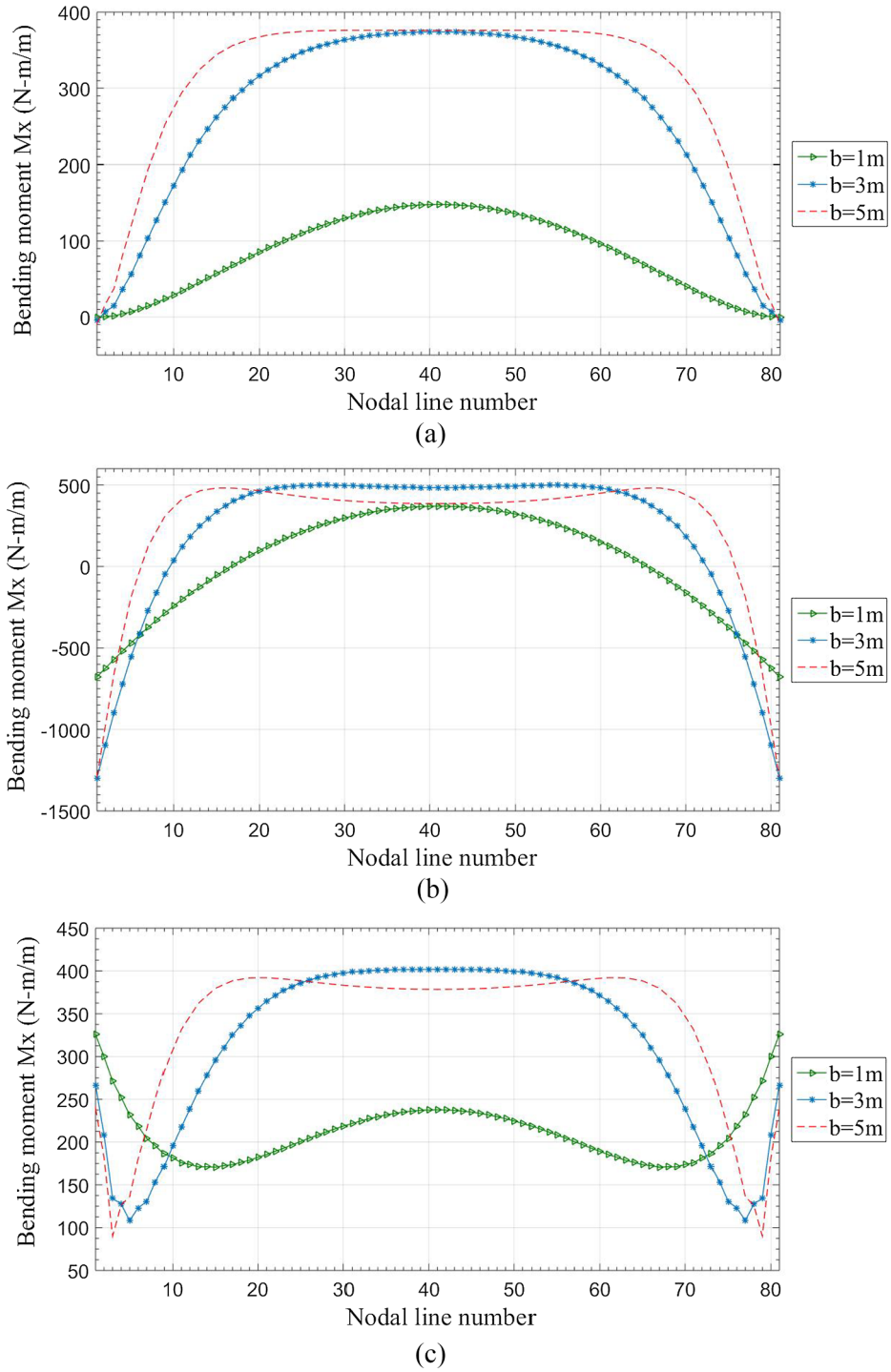

Fig. 12. Bending moment M_x in the middle of CSPs along the transverse direction for different widths and (a) FSFS, (b) CSCS, and (c) GSGS boundary conditions.

the plate with FSFS boundary conditions. As expected, the bending moments in free boundaries are zero. To compare the effect of boundary conditions, the bending moment diagrams for CSCS and GSGS boundary conditions are also presented in Fig. 12b and 12c.

4.3.3.2. CC transverse edges. The moment diagrams of FCFC and CCCC boundary conditions are presented in Fig. 13a and b, respectively. As for the FCFC plate, the finite strip method cannot capture the exact behavior of the plate in free boundaries. Therefore, the bending moment at these points is not exactly equal to zero as shown in Fig. 13a. According to Fig. 13b, it is shown that despite the greater stiffness of the supports in CCCC CSP, the positive moments in this case are smaller compared to SSSS and CSCS boundary conditions. The reasons of this behavior are the smaller displacements of CCCC CSPs, and also the different distribution of moments in different parts of the plate. Just like a beam that undergoes a higher positive moment in simply supports conditions rather than the both-end fixed supports.

4.4. Vibration analysis

After a comprehensive static analysis, the free and forced vibrations of the corrugated-core sandwich plate are now presented. In this

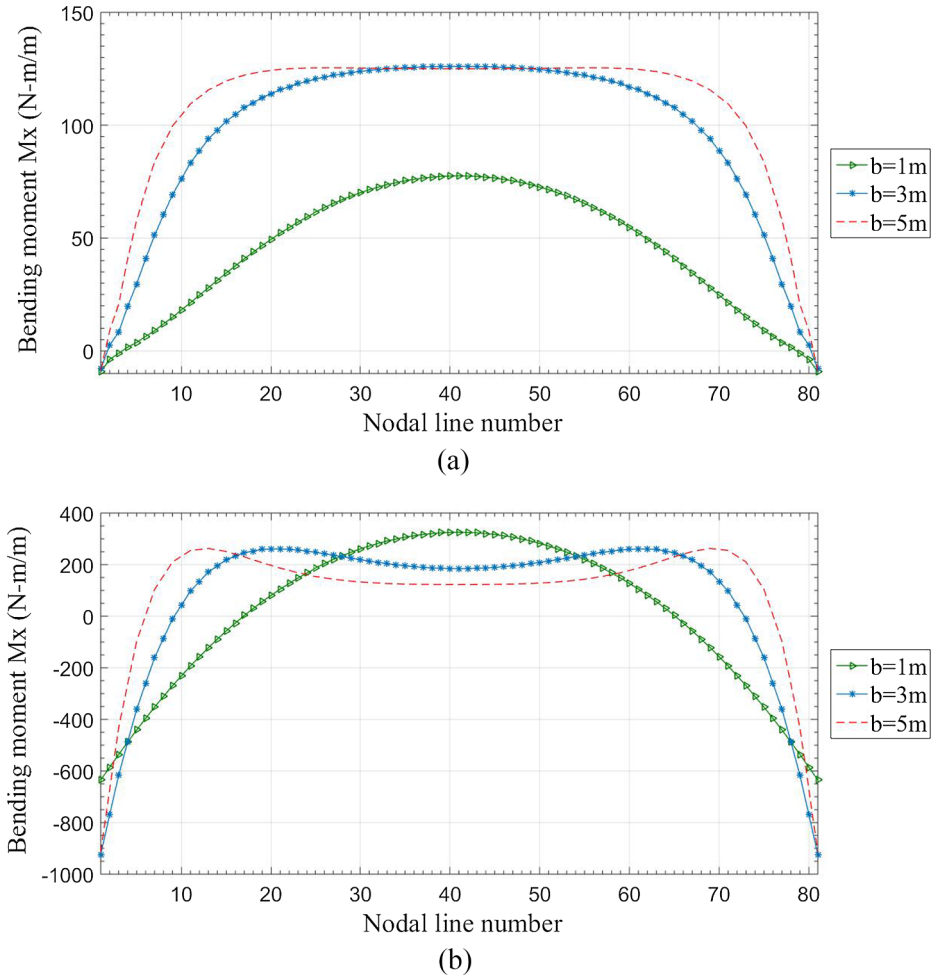

Fig. 13. Bending moment M_x in the middle of CSPs along the transverse direction for different widths and (a) FCFC and (b) CCCC boundary conditions.

section, the equivalent density of the orthotropic plate is assumed to be equal to$\rho A_c/2Ph_t$in which the cross section area of each unit of the plate, A_c, is calculated by Eq. (38) and other parameters are already defined.

$$\mathrm{A}_c = 4\theta R_c t_c + 2ft_c + 4d_1 t_c + 4Pt_f \tag{38}$$

The equivalent method proposed in Ref. [8] does not clearly restrict the nature of the applied forces to the static ones. Obtaining the equivalent elastic constants is somehow similar to determining the stiffness of a frame before dynamic analysis. Therefore, by assuming the dynamic loading as a chain of quasi-static loadings, the equivalent elastic constants could be used to approximate the dynamic results. As long as the constituent elements of the plate are not ruptured by the effect of dynamic loadings, one can use the elastic constants as an approximation of the stiffness of the structure.

The variations of λ versus length to width ratio for five different inclination angles and different boundary conditions are presented in Fig. 14a to d. Wherever the overall stiffness of the plate is higher, the natural frequency will have higher values, hence in smaller inclination angles, the values of λ are higher. Also, the natural frequencies are higher for clamped boundary conditions rather than the other ones with the same geometric parameters. Obviously, in the FSFS case, the results will have the lowest values. All of the graphs in Fig. 14 show that the natural frequencies converge to approximately constant values after certain lengths.

In the state of forced vibration, the plate is supposed to be under harmonic uniformly distributed loading$P_0 \sin(\omega t)$. Different loading frequencies are considered and the ratios of dynamic displacements to the static ones, w_{dyn}/w_{st}, are computed and the results are presented in Fig. 15 in the form of FRF diagrams for two types of boundary conditions. The diagrams are illustrated for CSPs with 1 m width during one second of vibration. Ten harmonic modes were employed for these calculations. It is observed that the plate responses can be far different from static results due to resonance effect which depends on the natural frequency of the plate. As the dimensions of the plate are increased, the natural frequencies become smaller and the resonance takes place at lower frequencies.

The maximum displacement diagrams of square CSPs with 1 m length and $\omega = 1000$ rad/sec for different inclination angles and different web heights are plotted in Figs. 16 and 17, respectively. The variation of overall stiffness of the corrugated sandwich plate (whether by changing in boundary condition or the geometric parameters) influences the stiffness matrix, natural frequencies, and even the equivalent density of the plate in the cases that the geometric parameters of the cross section change.

5. Conclusion

In this paper, a systematic static and dynamic analysis of corrugated-core sandwich plates was carried out using the classic finite strip method. The effects of geometric parameters such as dimensions, the inclination angle of the core plate, the width of each unit, the height of the web and boundary conditions on the behavior of corrugated sandwich plates under static and dynamic loadings were investigated and the results were presented in the form of figures and tables.

The concluding marks are listed as follows:

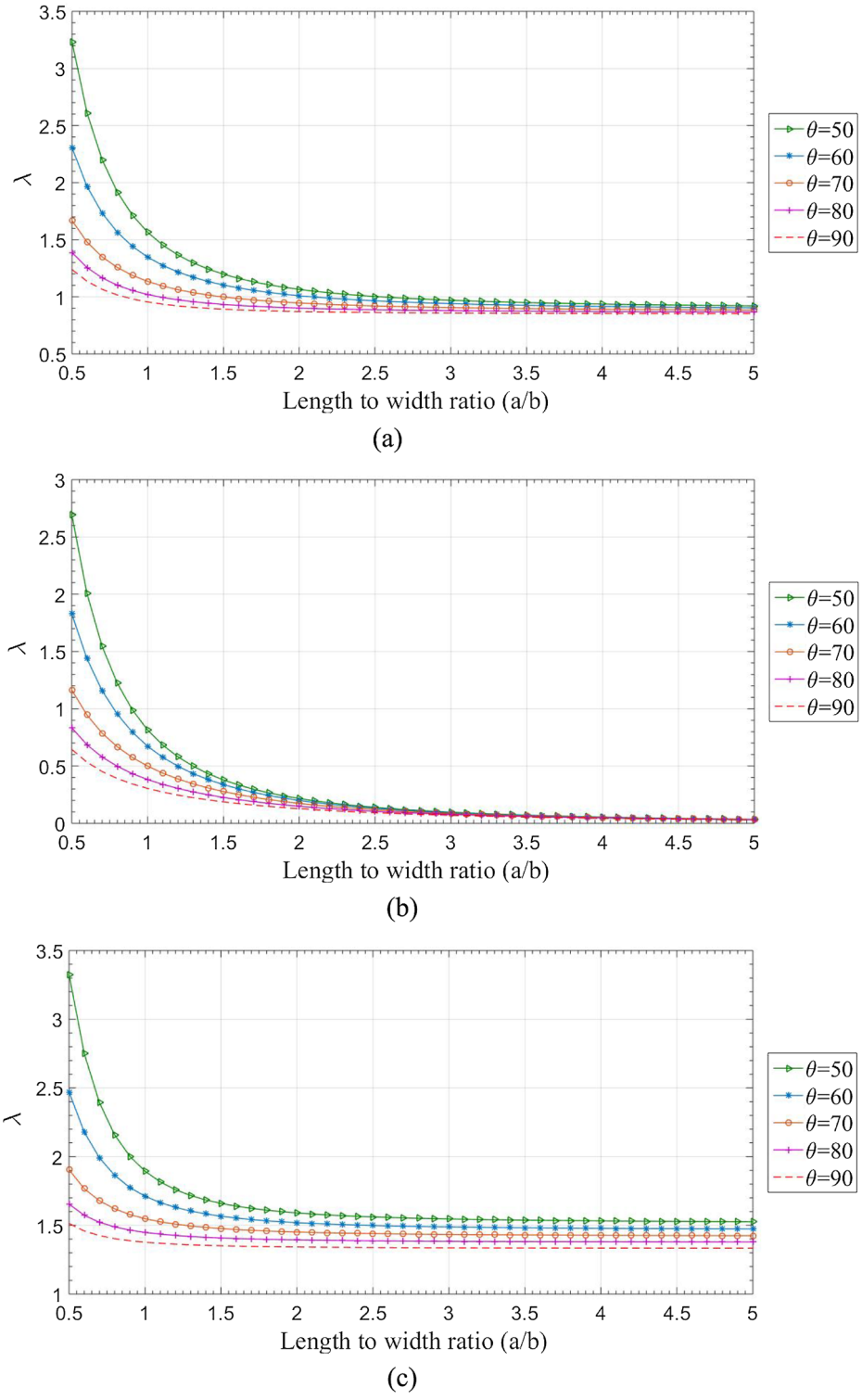

Fig. 14. The non-dimensional frequency factor, λ, of CSPs versus aspect ratio for different inclination angles and (a) SSSS, (b) FSFS, (c) CSCS, and (d) CCCC boundary conditions.

1. The increase in the arc of the core plate reduces the displacements.
2. To reduce the displacements, increasing the thickness of the face plates is generally more effective than increasing the thickness of the core plate.
3. Increasing the inclination angle, slightly increases the flexural stiffness, but reduces the shear stiffness, particularly D_{qy}, which eventually increases the displacements of the plate.
4. Increasing the width of each unit of the plate causes a slight increase in flexural stiffnesses and a significant reduction in shear stiffness, which eventually increases the displacements of the plate without having much effect on the economic aspects of the design.
5. Due to the high sensitivity of overall behavior of CSP to the core performance, the use of stronger materials in the face plate does not necessarily lead to a significant reduction in displacements of the plate.
6. The sign of nodal rotations ψ_y could change in the plates which have

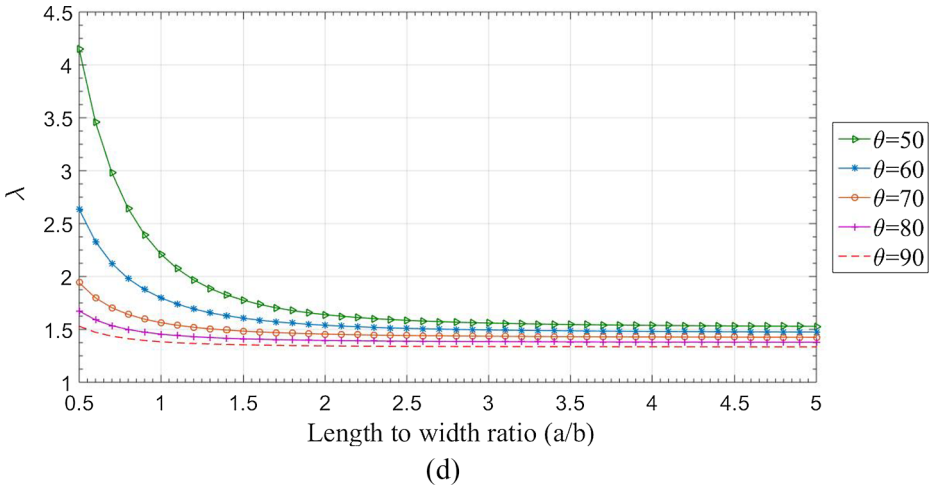

(d)

Fig. 14. (*continued*)

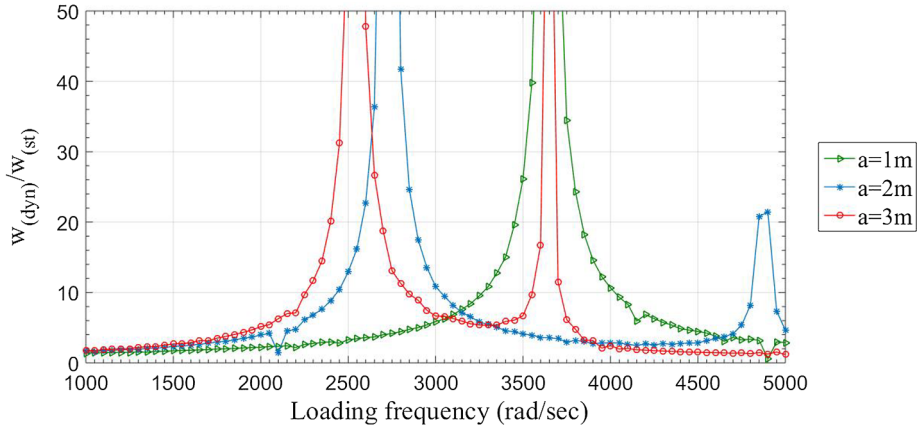

(a)

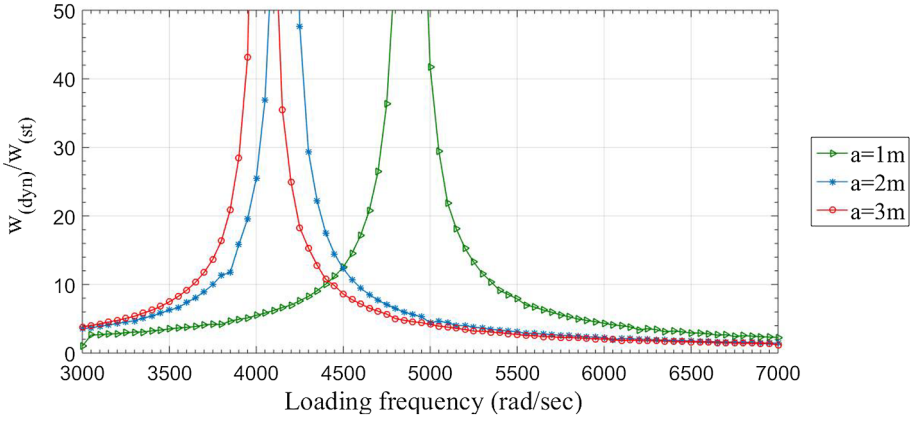

(b)

Fig. 15. Frequency response function diagrams of CSPs for different lengths: (a) SSSS and (b) CCCC boundary conditions.

relatively small shear to flexural stiffness values.

7. Due to the orthotropic nature of the CSPs, bending moments are different in two orthogonal directions. The flexural moment developed in the plate in different inclination angles are different, and the trends of variation of M_x and $M_y$with inclination angles are different from each other.
8. The displacement values in a plate under dynamic loading depends -in addition to the load intensity- on the loading frequency and the ratio of this frequency to the values of natural frequency of the plate. The free vibration frequency and the equivalent density of the plate vary with the variation of its geometry and affect the responses.

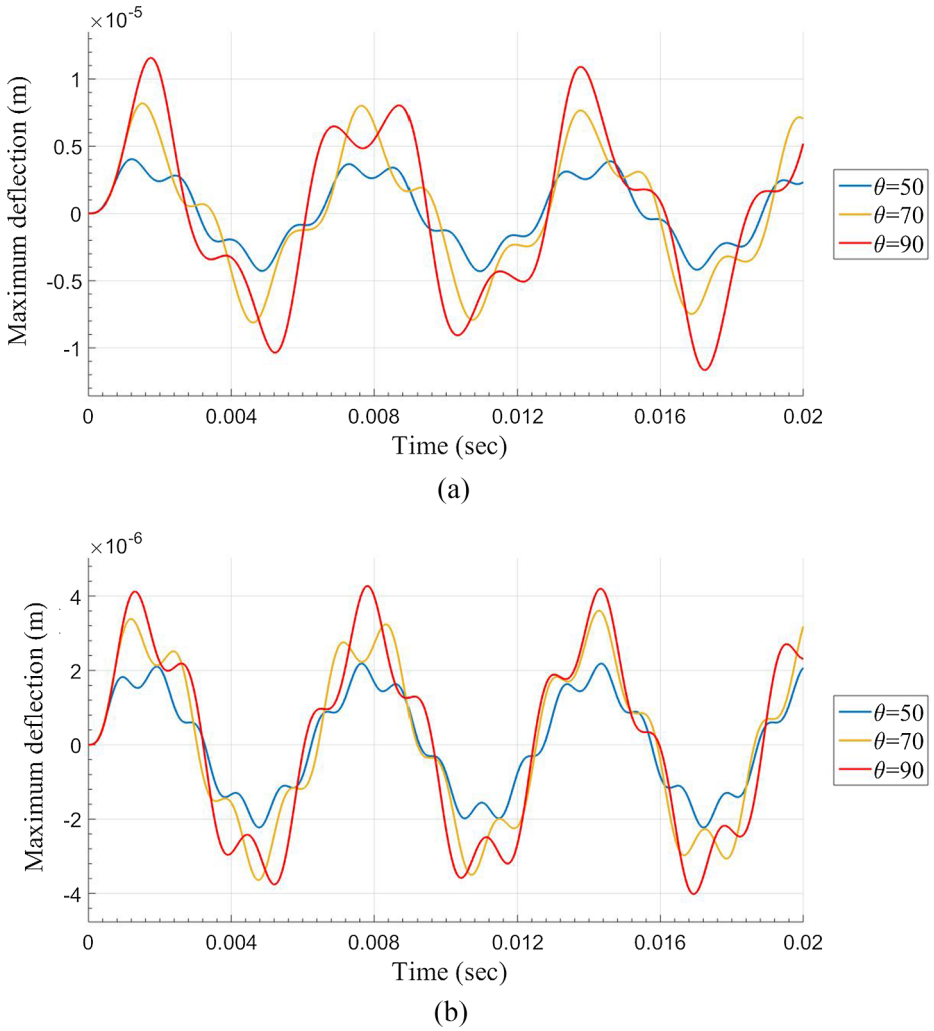

Fig. 16. Maximum deflections of CSP under harmonic loading (ω = 1000 rad/sec) for different inclination angles: (a) SSSS and (b) CCCC boundary conditions.

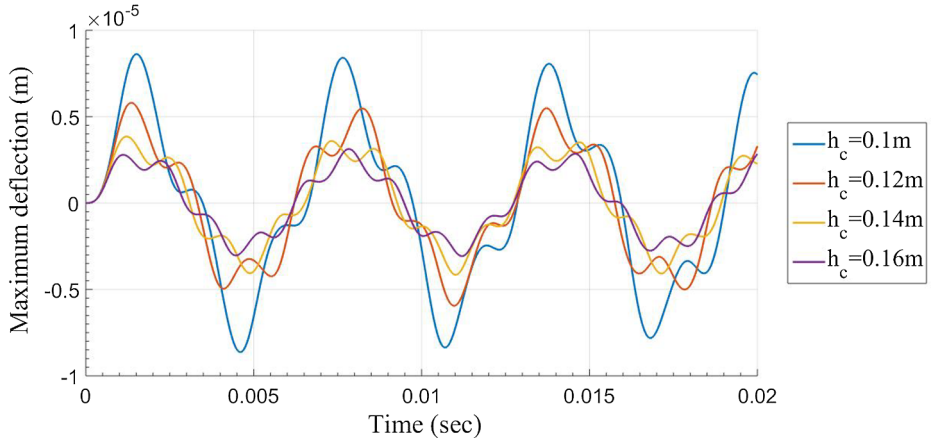

Fig. 17. Maximum deflections of SSSS CSPs under harmonic loading (ω = 1000 rad/sec) for different web heights.

Appendix

The non-dimensional parameter, S, in Eq. (6) is calculated as follows:

$$S = \frac{6\frac{h_c}{P}B_3B_7 + \left(\frac{P}{h_c}\right)^2}{12\left[-2\left(\frac{P}{h_c}\right)^2 B_4 + \frac{h_c}{h}\left[6B_7(B_3B_6 - B_4^2) + \left(\frac{P}{h_c}\right)^3 B_6\right] + \left(\frac{hP}{h_c^2}\right)B_3\right]} \tag{A1}$$

in which the B_i coefficients can be obtained as follows:

$$B_3 = K_{IZ} + \frac{K_{LZ}}{12}\left(\frac{t_c}{h_c}\right)^2 \tag{A2}$$

$$B_4 = K_{IYZ} - \frac{K_{LYZ}}{12}\left(\frac{t_c}{h_c}\right)^2 \tag{A3}$$

$$B_6 = K_{IY} + \frac{K_{LY}}{12}\left(\frac{t_c}{h_c}\right)^2 \tag{A4}$$

$$B_7 = \frac{E_f}{E_c}\left(\frac{1-v_c^2}{1-v_f^2}\right)\left(\frac{t_f}{t_c}\right)^3 \tag{A5}$$

where

$$K_{IZ} = \frac{1}{h_c}\int y^2 ds = \left(\frac{2d_1}{3h_c}\right)\left(\frac{k_1}{h_c}\right)^2 + \frac{2}{3}\left[\frac{1}{8}\left(\frac{P}{h_c}\right)^3 - \left(\frac{b_1}{h_c}\right)^3\right] + 2\left(\frac{R_c}{h_c}\right)\left\{\frac{b_1}{h_c}\left[\frac{\theta b_1}{h_c} - 2\left(\frac{R_c - e_1}{h_c}\right)\right] + \frac{1}{2}\left[\theta\left(\frac{R_c}{h_c}\right)^2 - \frac{g_1 e_1}{h_c^2}\right]\right\} \tag{A6}$$

$$K_{IYZ} = \frac{1}{h_c^3}\int yz ds = \frac{2j_1 k_1 d_1}{3h_c^3} + \frac{1}{2}\left[\frac{1}{4}\left(\frac{P}{h_c}\right)^2 - \left(\frac{b_1}{h_c}\right)^2\right] + 2\left(\frac{R_c}{h_c}\right)\left[\left(\frac{a_1}{h_c}\right)\left(\theta\frac{b_1}{h_c} + \frac{e_1}{h_c} - \frac{R_c}{h_c}\right) + \left(\frac{g_1}{h_c}\right)\left(\frac{b_1}{h_c} - \frac{g_1}{2h_c}\right)\right] \tag{A7}$$

$$K_{IY} = \frac{1}{h_c^3}\int z^2 ds = \frac{2d_1}{3h_c}\left(\frac{j_1}{h_c}\right)^2 + \frac{f}{4h_c} + 2\left(\frac{R_c}{h_c}\right)\left[\left(\frac{a_1}{h_c}\right)\left(\theta\frac{a_1}{h_c} + 2\frac{g_1}{h_c}\right) + \frac{1}{2}\left(\theta\left(\frac{R_c}{h_c}\right)^2 + \frac{g_1 e_1}{h_c^2}\right)\right] \tag{A8}$$

$$K_{LY} = \frac{1}{h_c}\int \cos^2(\psi) ds = \frac{f}{h_c} + \frac{2d_1\cos^2(\theta)}{h_c} + \frac{R_c}{h_c}[\theta + \cos(\theta)\sin(\theta)] \tag{A9}$$

$$K_{LYZ} = \frac{1}{h_c}\int \cos(\psi)\sin(\psi) ds = 2\frac{d_1\cos(\theta)\sin(\theta)}{h_c} + \frac{R_c\sin^2(\theta)}{h_c} \tag{A10}$$

$$K_{LZ} = \frac{1}{h_c}\int \sin^2(\psi)\, ds = \frac{2d_1\sin^2(\theta)}{h_c} + R_c\left[\frac{\theta - \cos(\theta)\sin(\theta)}{h_c}\right] \tag{A11}$$

$$K_L = \frac{1}{h_c}\int ds = 2\frac{d_1}{h_c} + 2\theta\frac{R_c}{h_c} + \frac{f}{h_c} \tag{A12}$$

In these equations, ψ is the angle between each part of one leg of the core plate (including the horizontal, oblique and arched parts of the core plate) and the horizontal line. Other geometric parameters in this section are shown in Fig. 2a and b.

References

[1] Carta G, Brun M, Movchan AB, Movchan NV, Jones IS. Dispersion properties of vortex-type monatomic lattices. Int J Solids Struct 2014;51(11–12):2213–25.
[2] Gonella S, Ruzzene M. Analysis of in-plane wave propagation in hexagonal and re-entrant lattices. J Sound Vib 2008;312(1–2):125–39.
[3] Krattiger D, Khajehtourian R, Bacquet CL, Hussein MI. Anisotropic dissipation in lattice metamaterials. AIP Adv 2016;6(12):121802.
[4] Wang Y-Z, Wang Y-S. Active control of elastic wave propagation in nonlinear phononic crystals consisting of diatomic lattice chain. Wave Motion 2018;78:1–8.
[5] Gough G, Elam C, Tipper G, De Bruyne N. The stabilisation of a thin sheet by a continuous supporting medium. Aeronaut J 1940;44(349):12–43.
[6] Williams D, Leggett D, Hopkins HG. Flat Sandwich Panels Under Compressive End Loads. HM Stationery Office; 1941.
[7] Libove C, Batdorf S. A general small-deflection theory for flat sandwich plates. Book A general small-deflection theory for flat sandwich plates, Series A general small-deflection theory for flat sandwich plates. ed., Editor ed.^eds., DTIC Document; 1948, pp.
[8] Libove C, Hubka RE. Elastic constants for corrugated-core sandwich plates vol. No. pp. 1951.
[9] Caillerie D, Nedelec J. Thin elastic and periodic plates. Math Methods Appl Sci 1984;6(1):159–91.
[10] Bourgeois S, Cartraud P, Debordes O. Homogenization of Periodic Sandwiches, Mechanics of Sandwich Structures. Springer; 1998. p. 131–8.
[11] Fung T-C, Tan K, Lok T. Shear stiffness DQy for C-core sandwich panels. J Struct Eng 1996;122(8):958–66.
[12] Fung T-C, Tan K-H, Lok T-S. Elastic constants for Z-core sandwich panels. J Struct Eng 1994;120(10):3046–55.
[13] He L, Cheng Y-S, Liu J. Precise bending stress analysis of corrugated-core, honeycomb-core and X-core sandwich panels. Compos Struct 2012;94(5):1656–68.
[14] Lok T-S, Cheng Q-H. Elastic stiffness properties and behavior of truss-core sandwich panel. J Struct Eng 2000;126(5):552–9.
[15] Liang C-C, Yang M-F, Wu P-W. Optimum design of metallic corrugated core sandwich panels subjected to blast loads. Ocean Eng 2001;28(7):825–61.
[16] Chang W.-S. Elasto-plastic analysis of corrugated sandwich steel panels. Vol. No. pp. 2004.
[17] Buannic N, Cartraud P, Quesnel T. Homogenization of corrugated core sandwich panels. Compos Struct 2003;59(3):299–312.
[18] Biancolini M. Evaluation of equivalent stiffness properties of corrugated board. Compos Struct 2005;69(3):322–8.
[19] Isaksson P, Krusper A, Gradin PA. Shear correction factors for corrugated core structures. Compos Struct 2007;80(1):123–30.
[20] Seong DY, Jung CG, Yang DY, Moon KJ, Ahn DG. Quasi-isotropic bending responses of metallic sandwich plates with bi-directionally corrugated cores. Mater Des 2010;31(6):2804–12.
[21] Bartolozzi G, Baldanzini N, Pierini M. Equivalent properties for corrugated cores of sandwich structures: a general analytical method. Compos Struct 2014;108:736–46.
[22] Boorle RK, Mallick PK. Global bending response of composite sandwich plates with corrugated core: Part I: effect of geometric parameters. Compos Struct 2016;141:375–88.
[23] Lok T-S, Cheng Q-H. Free and forced vibration of simply supported, orthotropic sandwich panel. Comput Struct 2001;79(3):301–12.
[24] Peng L-X, Yan S-T, Mo G-K, Zhang X. Free vibration analysis of corrugated-core sandwich plates using a meshfree Galerkin method based on the first-order shear deformation theory. Int J Mech Sci 2014;78:8–18.

[25] Mindlin RD, Influence of rotary inertia and shear on flexural motions of isotropic elastic plates. vol. No. pp. 1951.
[26] Reissner E. The effect of transverse shear deformation on the bending of elastic plates. J Appl Mech 1945;No:A69–77.
[27] Cheung Y. The finite strip method in the analys of elastic plates with two opposite simply supported ends. Proc Inst Civ Eng 1968;40(1):1–7.
[28] Cheung Y, Tham L, Li W. Free vibration and static analysis of general plate by spline finite strip. Comput Mech 1988;3(3):187–97.
[29] Cheung Y-K, Cheung MS. Flexural vibrations of rectangular and other polygonal plates. J Eng Mech Div 1971;97(2):391–411.
[30] Gay D, Gambelin J. Modeling and dimensioning of structures: a practical approach. Wiley Online Library; 2008.
[31] Liew K, Xiang Y, Kitipornchai S. Transverse vibration of thick rectangular plates—I. Comprehensive sets of boundary conditions. Comput Struct 1993;49(1):1–29.